SIAM J. IMAGING SCIENCES
Vol. 7, No. 2, pp. 1210–1236

Role of Scattering in Virtual Source Array Imaging*

Josselin Garnier† and George Papanicolaou‡

Abstract. We consider imaging in a scattering medium where the illumination goes through this medium but there is also an auxiliary, passive receiver array that is near the object to be imaged. Instead of imaging with the source-receiver array on the far side of the object, we image with the data of the passive array on the near side of the object. The imaging is done with travel time migration using the cross correlations of the passive array data. We showed in [J. Garnier and G. Papanicolaou, *Inverse Problems*, 28 (2012), 075002] that if (i) the source array is infinite, (ii) the scattering medium is modeled by either an isotropic random medium in the paraxial regime or a randomly layered medium, and (iii) the medium between the auxiliary array and the object to be imaged is homogeneous, then imaging with cross correlations completely eliminates the effects of the random medium. It is as if we imaged with an active array, instead of a passive one, near the object. The purpose of this paper is to analyze the resolution of the image when both the source array and the passive receiver array are finite. We show with a detailed analysis that for isotropic random media in the paraxial regime, not only is imaging not affected by the inhomogeneities, but the resolution can in fact be enhanced. This is because the random medium can increase the diversity of the illumination. We also show analytically that this will not happen in a randomly layered medium, and there may be some loss of resolution in this case.

Key words. imaging, wave propagation, random media, cross correlation

AMS subject classifications. 35R60, 86A15

DOI. 10.1137/13094181X

1. Introduction.

In conventional active array imaging (see Figure 1, left), the sources are on an array located at $(\vec{\boldsymbol{x}}_s)_{s=1}^{N_{\rm s}}$, the receivers are at $(\vec{\boldsymbol{x}}_r)_{r=1}^{N_{\rm r}}$, and the two arrays are coincident. The array response matrix is given by

$$\big\{p(t,\vec{\boldsymbol{x}}_r;\vec{\boldsymbol{x}}_s),\, t\in\mathbb{R},\, r=1,\ldots,N_{\rm r},\, s=1,\ldots,N_{\rm s}\big\} \tag{1.1}$$

and consists of the signals recorded by the rth receiver when the sth source emits a short pulse. An image is formed by migrating the array response matrix. The Kirchhoff migration imaging function [3, 4] at a search point $\vec{\boldsymbol{y}}^S$ in the image domain is given by

$$\mathcal{I}(\vec{\boldsymbol{y}}^S)=\frac{1}{N_{\rm s}N_{\rm r}}\sum_{r=1}^{N_{\rm r}}\sum_{s=1}^{N_{\rm s}}p\Big(\frac{|\vec{\boldsymbol{x}}_s-\vec{\boldsymbol{y}}^S|+|\vec{\boldsymbol{y}}^S-\vec{\boldsymbol{x}}_r|}{c_0},\vec{\boldsymbol{x}}_r;\vec{\boldsymbol{x}}_s\Big). \tag{1.2}$$

*Received by the editors October 18, 2013; accepted for publication (in revised form) March 24, 2014; published electronically June 3, 2014.
http://www.siam.org/journals/siims/7-2/94181.html

†Laboratoire de Probabilités et Modèles Aléatoires & Laboratoire Jacques-Louis Lions, Université Paris Diderot, 75205 Paris Cedex 13, France (garnier@math.univ-paris-diderot.fr). The work of this author was partially supported by ERC Advanced Grant Project MULTIMOD-26718.

‡Mathematics Department, Stanford University, Stanford, CA 94305 (papanicolaou@stanford.edu). The work of this author was partially supported by AFOSR grant FA9550-11-1-0266.

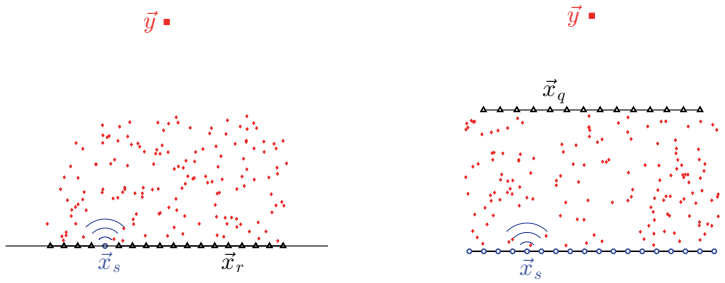

Figure 1. *Sensor array imaging of a reflector located at $\vec{\boldsymbol{y}}$ through a scattering medium. Left: Conventional imaging; $\vec{\boldsymbol{x}}_s$ is a source; $\vec{\boldsymbol{x}}_r$ is a receiver. Right: Use of an auxiliary passive array for imaging through a scattering medium; $\vec{\boldsymbol{x}}_s$ is a source; $\vec{\boldsymbol{x}}_q$ is a receiver located beyond the scattering medium.*

Here $|\vec{\boldsymbol{x}} - \vec{\boldsymbol{y}}|/c_0$ is a computed travel time between the points $\vec{\boldsymbol{x}}$ and $\vec{\boldsymbol{y}}$, corresponding to a homogeneous medium with constant propagation speed c_0. In this case the images produced by Kirchhoff migration, that is, the peaks of the imaging function $\mathcal{I}(\vec{\boldsymbol{y}}^S)$, can be analyzed easily. For a point reflector the range resolution is c_0/B, where B is the bandwidth of the probing pulse, the cross range resolution is $\lambda_0 L/a$, where λ_0 is the central wavelength of the pulse, L is the distance from the array to the reflector, and a is the size of the array. These are the well-known Rayleigh resolution limits [12, 15]. When, however, the medium is inhomogeneous, migration may not work well. In weakly scattering media the images can be stabilized statistically by using coherent interferometry [9, 10, 11, 6, 7], which is a special correlation-based imaging method. Statistical stability here means high signal-to-noise ratio for the imaging function. In strongly scattering media we may be able to obtain an image by using special signal processing methods [8], but often we cannot get any image at all because the coherent signals from the reflector received at the array are very weak compared to the backscatter from the medium.

Let us also consider the possibility of imaging with an auxiliary *passive* array, with sensors located at $(\vec{\boldsymbol{x}}_q)_{q=1}^{N_\mathrm{q}}$, and with the scattering medium in between it and the surface source-receiver array (see Figure 1, right). The signals recorded by the auxiliary array form the data matrix

$$\big\{p(t, \vec{\boldsymbol{x}}_q; \vec{\boldsymbol{x}}_s),\, t \in \mathbb{R},\, q = 1, \ldots, N_\mathrm{q},\, s = 1, \ldots, N_\mathrm{s}\big\}. \tag{1.3}$$

How can we use the auxiliary passive array to get an image, and will it help in mitigating the effects of the strong scattering between it and the active source-receiver array? If we think of the strong scattering as producing signals that appear to come from spatially dispersed, statistically independent noisy sources, then we are in a daylight imaging setup with ambient noise sources, which was analyzed in [20]. Daylight imaging here means illumination coming from behind the receiver array. By analogy with having illumination from N_s uncorrelated point sources at $(\vec{\boldsymbol{x}}_s)_{s=1}^{N_\mathrm{s}}$, we expect that, even in the case of active impulsive sources, the matrix of cross correlations at the auxiliary array

$$\mathcal{C}\big(\tau, \vec{\boldsymbol{x}}_q, \vec{\boldsymbol{x}}_{q'}\big) = \sum_{s=1}^{N_\mathrm{s}} \int_{\mathbb{R}} p(t, \vec{\boldsymbol{x}}_q; \vec{\boldsymbol{x}}_s) p(t + \tau, \vec{\boldsymbol{x}}_{q'}; \vec{\boldsymbol{x}}_s) dt \tag{1.4}$$

will behave roughly as if it is the full active array response matrix of the auxiliary array, that is, the matrix of signals that would be obtained if the array consisted of $N_{\rm q}$ sources and receivers (hence the term "virtual sources"). This means that it can be used for imaging with Kirchhoff migration:

$$\mathcal{I}_{\rm C}(\vec{\boldsymbol{y}}^S) = \frac{1}{N_{\rm q}^2} \sum_{q,q'=1}^{N_{\rm q}} \mathcal{C}\Big(\frac{|\vec{\boldsymbol{x}}_q - \vec{\boldsymbol{y}}^S| + |\vec{\boldsymbol{y}}^S - \vec{\boldsymbol{x}}_{q'}|}{c_0}, \vec{\boldsymbol{x}}_q, \vec{\boldsymbol{x}}_{q'} \Big). \tag{1.5}$$

In our previous paper [22] we showed analytically the striking result that the resolution of the images obtained this way is given by the Rayleigh resolution formulas as if the medium were homogeneous [21]. This result is not obvious, simply because scattering by inhomogeneities of waves emitted by the impulsive sources at the surface produces signals on the auxiliary passive array that are very different from those coming from spatially uncorrelated noise sources. This is especially true when addressing randomly layered media, which do not provide any lateral diversity enhancement since scattering does not change the transverse wave vectors. Nevertheless, it has been anticipated and observed in exploration geophysics contexts [2, 30, 33] that imaging with the cross correlations of the auxiliary array is very effective and produces images that are nearly as good as in a homogeneous medium. We showed this for randomly layered media in the asymptotic regime studied in detail in [17] and for isotropic random media in the paraxial regime [31, 32, 27, 13, 24].

The reason why this kind of imaging works so well is because, by wave field reciprocity, the cross correlations $\mathcal{C}(\tau, \vec{\boldsymbol{x}}_q, \vec{\boldsymbol{x}}_{q'})$ can be given a time-reversal interpretation, a well-known [14] observation that we reproduce below, and then we can apply the analysis of time-reversal refocusing in random media [5, 17]. The main results in time reversal in random media are (i) the enhanced refocusing, which means that the primary peak in the cross correlation will be observable only when the sensors in the auxiliary array are close enough with time lag close to zero, and then Kirchhoff migration to image the reflector will not be affected, and (ii) the statistical stability of the cross correlation function relative to the random medium inhomogeneities, provided that the source illumination from the surface is broadband (see [17, Chapters 12 and 15] and [16, 18]).

The analysis carried out in this paper is based on the asymptotic expressions of the moments of the Green's function in the two regimes addressed in this paper. These expressions are not new and were used previously to analyze time-reversal experiments (see [28, 29] in the random paraxial regime and [18, 17] in the randomly layered regime). The enhanced resolution due to multiple scattering was known in the context of time reversal, but the imaging context considered in this paper is very different. In time reversal, the recorded signals are time-reversed and re-emitted into the medium by the time-reversal array; therefore, the waves propagate physically in the real medium and they can benefit from the multipathing induced by scattering. In classical imaging, the waves received at the array are backpropagated analytically or computationally in a synthetic homogeneous medium since the small medium fluctuations are not known. In this case the scattering effects (in particular the random phases) cannot be removed or mitigated during the backpropagation. It turns out that the backpropagation of the cross correlation matrix of the array data in the synthetic medium can benefit from the multiply scattered wave components, provided that multiple scattering

has good isotropic properties. This insight in the context of imaging is new.

In the previous paragraph we emphasized that this paper is about imaging, in which backpropagation is carried out numerically in a synthetic homogeneous medium, and not about time reversal, in which backpropagation is carried out physically in the real medium. However, there is a relation between the two problems when cross correlations are used for imaging. Indeed, the cross correlation (1.4) has an interpretation in terms of a time-reversal experiment: If we consider that the sources at $(\vec{\boldsymbol{x}}_s)_{s=1}^{N_{\rm s}}$ are pointlike, and if we use the reciprocity property of the Green's function, then the cross correlation can be written as

$$\mathcal{C}\big(\tau, \vec{\boldsymbol{x}}_q, \vec{\boldsymbol{x}}_{q'}\big) = \sum_{s=1}^{N_{\rm s}} \int_{\mathbb{R}} p(\tau - t, \vec{\boldsymbol{x}}_{q'}; \vec{\boldsymbol{x}}_s) p(-t, \vec{\boldsymbol{x}}_s; \vec{\boldsymbol{x}}_q) dt.$$

This is the field observed at $\vec{\boldsymbol{x}}_{q'}$ during a time-reversal experiment in the situation in which (1) an original source at $\vec{\boldsymbol{x}}_q$ emits a short pulse and (2) a time-reversal array at $(\vec{\boldsymbol{x}}_s)_{s=1}^{N_{\rm s}}$ records the waves, time-reverses them, and re-emits them into the same medium. This time-reversal interpretation of the cross correlation (1.4) explains why the tools used to analyze time reversal in the random paraxial regime or in the randomly layered regime are also appropriate to analyze cross correlation imaging.

In this paper we explore analytically the effect of finite array sizes in correlation-based imaging. We first formulate the direct scattering problem more precisely. The space coordinates are denoted by $\vec{\boldsymbol{x}} = (\boldsymbol{x}, z) \in \mathbb{R}^2 \times \mathbb{R}$. The waves are emitted by a point source located at $\vec{\boldsymbol{x}}_s$ which belongs to an array of sources $(\vec{\boldsymbol{x}}_s)_{s=1,\dots,N_{\rm s}}$ located in the plane $z = 0$. The waves are recorded by an array of receivers $(\vec{\boldsymbol{x}}_q)_{q=1,\dots,N_{\rm q}}$ located in the plane $z = L$ (see Figure 2). The recorded signals form the data matrix (1.3). The scalar wave field $(t, \vec{\boldsymbol{x}}) \mapsto p(t, \vec{\boldsymbol{x}}; \vec{\boldsymbol{x}}_s)$ satisfies the wave equation

$$\frac{1}{c(\vec{\boldsymbol{x}})^2} \frac{\partial^2 p}{\partial t^2} - \Delta p = -\nabla \cdot \vec{\boldsymbol{F}}(t, \vec{\boldsymbol{x}}; \vec{\boldsymbol{x}}_s), \tag{1.6}$$

where $c(\vec{\boldsymbol{x}})$ is the speed of propagation in the medium and the forcing term $(t, \vec{\boldsymbol{x}}) \mapsto \vec{\boldsymbol{F}}(t, \vec{\boldsymbol{x}}; \vec{\boldsymbol{x}}_s)$ models the source. It is pointlike, located at $\vec{\boldsymbol{x}}_s = (\boldsymbol{x}_s, 0)$, i.e., at the surface $z = 0$, and it emits a pulse:

$$\vec{\boldsymbol{F}}(t, \vec{\boldsymbol{x}}; \vec{\boldsymbol{x}}_s) = \vec{\boldsymbol{f}}(t) \delta(z) \delta(\boldsymbol{x} - \boldsymbol{x}_s). \tag{1.7}$$

We consider in this paper a randomly scattering medium that occupies the section $z \in (0, L)$ and is sandwiched between two homogeneous half-spaces:

$$\frac{1}{c(\vec{\boldsymbol{x}})^2} = \frac{1}{c_0^2}\big(1 + \mu(\vec{\boldsymbol{x}})\big), \qquad \vec{\boldsymbol{x}} \in \mathbb{R}^2 \times (0, L), \tag{1.8}$$

where $\mu(\vec{\boldsymbol{x}})$ is a zero-mean stationary random process modeling the random heterogeneities present in the medium.

We consider scattering by a reflector above the random medium placed at $\vec{\boldsymbol{y}} = (\boldsymbol{y}, L_y)$, $L_y > L$. The reflector is modeled by a local change of the speed of propagation of the form

$$\frac{1}{c(\vec{\boldsymbol{x}})^2} = \frac{1}{c_0^2}\Big(1 + \frac{\sigma_{\rm ref}}{|\Omega_{\rm ref}|} \mathbf{1}_{\Omega_{\rm ref}}(\vec{\boldsymbol{x}} - \vec{\boldsymbol{y}})\Big), \qquad \vec{\boldsymbol{x}} \in \mathbb{R}^2 \times (L, \infty), \tag{1.9}$$

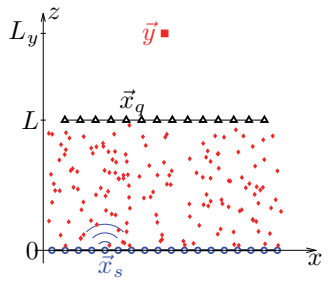

Figure 2. *Sensor array imaging of a reflector through a scattering medium in the region $z \in (0, L)$. $\vec{\boldsymbol{x}}_s$ is a source, $\vec{\boldsymbol{x}}_q$ is a receiver, and $\vec{\boldsymbol{y}}$ is the reflector.*

where $\Omega_{\rm ref}$ is a small domain and $\sigma_{\rm ref}$ is the reflectivity of the reflector.

The recorded signals form the data matrix (1.3). The goal is to extract the location of the reflector from the data. We will study the imaging function (1.5), considered in [22], that migrates the cross correlation of the recorded signals (1.4). In [22] we analyzed the case in which the source array has full aperture, which means that it extends over the whole surface $z = 0$. In this case we have shown both in the weakly scattering paraxial regime and in strongly scattering layered media that the correlation-based imaging function (1.5) produces images as if the medium between the sources and the receiver array were homogeneous and the receiver array were an active one made up of both sources and receivers. This imaging method turns out to be very efficient as it completely cancels the effect of random scattering.

In this paper we address the case in which the source array has finite aperture, which means that the sources do not extend over the whole surface $z = 0$. In this case it turns out that random scattering affects the resolution of the image, which is not the same with and without random scattering. However, the effect of random scattering depends on its angular properties, and it may enhance or reduce the isotropy of the illumination, which in turn enhances or reduces the resolution of the imaging function (1.5). We will analyze in detail the weakly scattering paraxial regime, for which random scattering is good for imaging, and the strongly scattering layered regime, for which random scattering is bad for imaging.

2. Summary of the results. We can give a simple explanation for why the imaging function (1.5) gives a good image provided that some ideal conditions are fulfilled. If the sources are pointlike, generate Dirac-like pulses, and densely surround the region of interest Ω, inside of which are the reflector and the receiver array, then we have

$$\hat{\mathcal{C}}(\omega, \vec{\boldsymbol{x}}_q, \vec{\boldsymbol{x}}_{q'}) = \int_{\partial\Omega} \hat{G}(\omega, \vec{\boldsymbol{x}}_q; \vec{\boldsymbol{x}}_s)\overline{\hat{G}(\omega, \vec{\boldsymbol{x}}_{q'}; \vec{\boldsymbol{x}}_s)}d\sigma(\vec{\boldsymbol{x}}_s),$$

where $\hat{G}(\omega, \vec{\boldsymbol{x}}_q; \vec{\boldsymbol{x}}_s)$ is the exact time-harmonic Green's function for the wave equation (1.6) including the reflector. In this paper the Fourier transform of a function $f(t)$ is defined by

$$\hat{f}(\omega) = \int f(t)e^{i\omega t}dt.$$

By the Helmholtz–Kirchhoff identity [20, 33], we find that, provided Ω is a ball with large radius,

$$\hat{C}(\omega, \vec{\boldsymbol{x}}_q, \vec{\boldsymbol{x}}_{q'}) = \frac{\omega}{c_0} \mathrm{Im}\big(\hat{G}(\omega, \vec{\boldsymbol{x}}_q; \vec{\boldsymbol{x}}_{q'})\big).$$

This shows that the cross correlation of the signals at two receivers $\vec{\boldsymbol{x}}_q$ and $\vec{\boldsymbol{x}}_{q'}$ looks like the signal recorded at $\vec{\boldsymbol{x}}_q$ when $\vec{\boldsymbol{x}}_{q'}$ is a source. Therefore, Kirchhoff migration of the cross correlation matrix should give a good image. The use of the Helmholtz–Kirchhoff identity gives the desired result, but it obscures the important role of scattering when the source array has finite aperture. We will show in this paper that it is not required to have a source array with full aperture to get a good image with the imaging function (1.5), but this result requires a deeper mathematical analysis than the often-used Helmholtz–Kirchhoff identity.

Let us briefly consider the situation shown in Figure 2, when the source array has full aperture and covers the surface $z = 0$, the angular illumination of the reflector is ultrawide, and the illumination cone covers the receiver array. This situation was analyzed in detail in [22]. In this case the correlation-based imaging function (1.5) completely cancels the effect of random scattering, and the results are equivalent regardless of the form of the scattering medium. The cross-range resolution of the imaging function is given by the classical Rayleigh resolution formula $\lambda_0(L_y - L)/a$, where a is the receiver array diameter. The range resolution is limited by the noise source bandwidth B and given by c_0/B.

The results are quite different when the source array has finite aperture and diameter b. In this case scattering turns out to play a critical role, as it may enhance or reduce the angular diversity of illumination of the reflector. This was already noticed in time reversal [14, 5, 17]: When waves emitted by a point source and recorded by an array are time-reversed and re-emitted into the medium, the time-reversed waves refocus at the original source location, and refocusing is enhanced in a scattering medium compared to a homogeneous one. This is because of the multipathing induced by scattering which enhances the refocusing cone. However, this is the first time in which this result is clearly seen in an imaging context, in which the backpropagation step is carried out numerically in a fictitious homogeneous medium, and not in the physical medium. This requires the backpropagation of the cross correlations of the recorded signals, and not the signals themselves.

We first address the case of a medium with isotropic three-dimensional weak fluctuations $\mu(\vec{\boldsymbol{x}})$ of the index of refraction. When the conditions for the paraxial approximation are fulfilled, backscattering can be neglected, and wave propagation is governed by a Schrödinger-type equation with a random potential that has the form of a zero-mean Gaussian field whose covariance function is given by

$$\mathbb{E}\big[B(\boldsymbol{x}, z)B(\boldsymbol{x}', z')\big] = \gamma_0(\boldsymbol{x} - \boldsymbol{x}')\big(z \wedge z'\big), \tag{2.1}$$

with

$$\gamma_0(\boldsymbol{x}) = \int_{-\infty}^{\infty} \mathbb{E}[\mu(\mathbf{0}, 0)\mu(\boldsymbol{x}, z)]dz. \tag{2.2}$$

We will show in section 3, by using multiscale analysis, that the cone of incoherent waves that illuminates the reflector is enhanced compared to the cone of coherent waves that illuminates

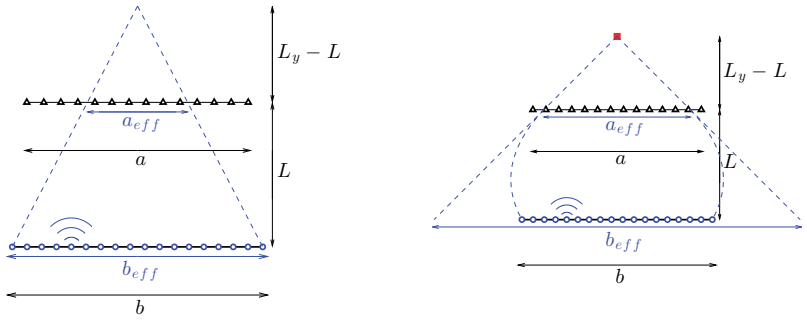

Figure 3. *If the medium is homogeneous (left picture), the illumination cone is determined by the physical source array diameter $b_{\rm eff} = b$. In the random paraxial regime (right picture), the angular diversity of the waves that illuminate the reflector is increased by scattering, and the effective illumination cone is enhanced and corresponds to an effective source array diameter $b_{\rm eff} > b$.*

the reflector through a homogeneous medium (see Figure 3), and this angular cone corresponds to an effective source array diameter $b_{\rm eff}$ given by

$$b_{\rm eff}^2 = b^2 + \frac{\bar{\gamma}_2 L^3}{3}, \tag{2.3}$$

where we have assumed that the correlation function γ_0 can be expanded as $\gamma_0(\boldsymbol{x}) = \gamma_0(\mathbf{0}) - \bar{\gamma}_2|\boldsymbol{x}|^2 + o(|\boldsymbol{x}|^2)$ for $|\boldsymbol{x}| \ll 1$. This in turn corresponds to an effective receiver array diameter $a_{\rm eff}$ (defined as the intersection of the illumination cone with the receiver array) given by

$$a_{\rm eff} = b_{\rm eff}\frac{L_y - L}{L_y}. \tag{2.4}$$

As a result, the cross-range resolution of the imaging function is given by the effective Rayleigh resolution formula $\lambda_0(L_y - L)/a_{\rm eff}$, which exhibits a resolution enhancement since $a_{\rm eff}$ is larger in a random medium than in a homogeneous one. The range resolution is still given by c_0/B. The detailed analysis is in subsection 3.4.

We next analyze the case of a medium with one-dimensional (layered) fluctuations $\mu(z)$ of the index of refraction. In this case it is known [17] that the scattering regime is characterized by strong backscattering and wave localization, with the localization length given by

$$L_{\rm loc} = \frac{4c_0^2}{\gamma\omega_0^2}, \tag{2.5}$$

where ω_0 is the noise source central frequency and

$$\gamma = \int_{-\infty}^{\infty} \mathbb{E}[\nu(z')\nu(z'+z)]dz \tag{2.6}$$

is the integrated covariance of the fluctuations of the index of refraction. We will show in section 4 that the cone of incoherent waves that illuminates the reflector is reduced compared

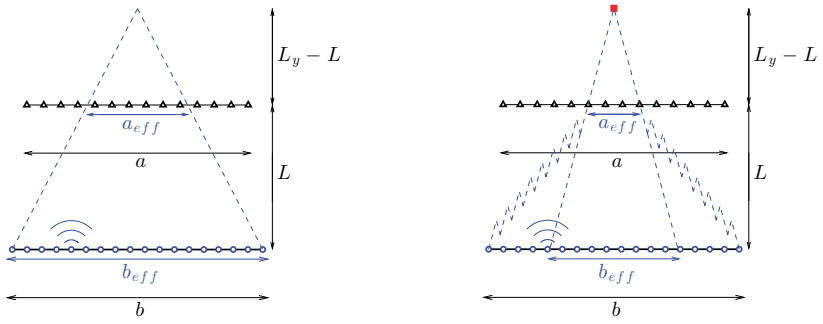

Figure 4. *If the medium is homogeneous (left picture), the illumination cone is determined by the physical source array diameter $b_{\text{eff}} = b$. If the medium is randomly layered (right picture), the angular diversity of the waves that illuminate the reflector is reduced by scattering (only the waves with wavevectors close to the vertical direction can reach the reflector after multiple scattering events that conserve the wavevectors in the layered case) and the effective illumination cone is reduced and corresponds to an effective source array diameter $b_{\text{eff}} < b$.*

to the cone of coherent waves that illuminates the reflector through a homogeneous medium (see Figure 4), because scattering does not change the transverse wavevector, and this angular cone corresponds to an effective source array diameter b_{eff} given by

$$b_{\text{eff}}^2 = \frac{4L_y^2 L_{\text{loc}}}{L}, \tag{2.7}$$

where we have assumed that $b^2 \gg LL_{\text{loc}}$. This again corresponds to an effective receiver array diameter a_{eff} given by

$$a_{\text{eff}} = b_{\text{eff}} \frac{L_y - L}{L_y}. \tag{2.8}$$

As a result, the cross-range resolution of the imaging function is given by the effective Rayleigh resolution formula $\lambda_0(L_y - L)/a_{\text{eff}}$, which exhibits a resolution reduction since a_{eff} is smaller in a randomly layered medium than in a homogeneous medium. Furthermore, as wave scattering is strongly frequency-dependent, the effective bandwidth is reduced as well,

$$B_{\text{eff}} = \frac{B}{\sqrt{1 + \frac{B^2 L}{4\omega_0^2 L_{\text{loc}}}}}, \tag{2.9}$$

and the range resolution is given by c_0/B_{eff}.

The comparative analysis of the random paraxial regime and the randomly layered regime clearly exhibits the role of scattering in correlation-based virtual source imaging. With a source array with full aperture, scattering plays no role, as the illumination of the reflector is ultrawide regardless of the scattering regime. When the source array is limited, if scattering is isotropic, then it enhances the angular diversity of the illumination of the reflector and the resolution of the correlation-based imaging function. If it is anisotropic, then it reduces the

angular diversity of the illumination of the reflector and the resolution of the correlation-based imaging function.

We note, however, that a large physical source array and/or broadband sources are necessary to ensure the statistical stability of the imaging function. This has been already addressed in detail in different contexts in [7, 23].

3. Imaging through a random medium in the paraxial regime.

3.1. The paraxial scaling regime. In this section we analyze a scaling regime in which scattering is isotropic and weak, which allows us to use the random paraxial wave model to describe wave propagation in the scattering region. In this approximation, backscattering is negligible, but there is significant lateral scattering as the wave advances and over long propagation distances. Even though scattering is weak, its effects accumulate and can be a limiting factor in imaging and communications if not mitigated in some way. Wave propagation in random media in the paraxial regime has been used extensively in underwater sound propagation as well as in the microwave and optical contexts in the atmosphere [32, 31]. We formulate the regime of paraxial wave propagation in random media with a scaling of parameters that allows detailed and effective mathematical analysis [24]. It is described as follows.

(1) We assume that the correlation length l_c of the medium is much smaller than the typical propagation distance L. We denote by ε^2 the ratio between the correlation length and the typical propagation distance:

$$\frac{l_c}{L} \sim \varepsilon^2.$$

(2) We assume that the transverse width of the source R_0 and the correlation length of the medium l_c are of the same order. This means that the ratio R_0/L is of order ε^2. This scaling is motivated by the fact that, in this regime, there is a nontrivial interaction between the fluctuations of the medium and the wave.

(3) We assume that the typical wavelength λ is much smaller than the propagation distance L; more precisely, we assume that the ratio λ/L is of order ε^4:

$$\frac{\lambda}{L} \sim \varepsilon^4.$$

This high-frequency scaling $\lambda \ll R_0 \ll L$ is the classical paraxial regime in which the beam generated by the source propagates along a privileged direction and spreads out by diffractive effects, which are of order one provided $L\lambda/R_0^2$ is of order one.

(4) We assume that the typical amplitude of the random fluctuations of the medium is small. More precisely, we assume that the relative amplitude of the fluctuations is of order ε^3. This scaling has been chosen so as to obtain an effective regime of order one when ε goes to zero. That is, if the magnitude of the fluctuations is smaller than ε^3, then the wave would propagate as if the medium were homogeneous, while if the order of magnitude is larger, then the wave would not be able to penetrate the random medium. The scaling that we consider here corresponds to the physically most interesting situation where random effects play a significant role, quantifiable within the paraxial regime.

3.2. The random paraxial wave equation. We consider the time-harmonic form of the scalar wave equation

$$(\partial_z^2 + \Delta_\perp)\hat{p} + \frac{\omega^2}{c_0^2}\big(1 + \mu(\boldsymbol{x}, z)\big)\hat{p} = 0. \tag{3.1}$$

Here μ is a random process that models the three-dimensional spatial fluctuations of the medium properties. It is assumed to be a zero-mean and stationary process with mixing properties in the z-direction. In the high-frequency regime described above,

$$\omega \to \frac{\omega}{\varepsilon^4}, \qquad \mu(\boldsymbol{x}, z) \to \varepsilon^3 \mu\left(\frac{\boldsymbol{x}}{\varepsilon^2}, \frac{z}{\varepsilon^2}\right), \tag{3.2}$$

the rescaled function $\hat{\phi}^\varepsilon$ defined by

$$\hat{p}^\varepsilon(\omega, \boldsymbol{x}, z) = \exp\left(i\frac{\omega}{\varepsilon^4}\frac{z}{c_0}\right)\hat{\phi}^\varepsilon\left(\frac{\omega}{\varepsilon^4}, \frac{\boldsymbol{x}}{\varepsilon^2}, z\right) \tag{3.3}$$

satisfies

$$\varepsilon^4 \partial_z^2 \hat{\phi}^\varepsilon + \left(2i\frac{\omega}{c_0}\partial_z \hat{\phi}^\varepsilon + \Delta_\perp \hat{\phi}^\varepsilon + \frac{\omega^2}{\varepsilon c_0^2}\mu\left(\boldsymbol{x}, \frac{z}{\varepsilon^2}\right)\hat{\phi}^\varepsilon\right) = 0. \tag{3.4}$$

The ansatz (3.3) corresponds to an upgoing plane wave with a relatively slowly varying envelope. In the regime $\varepsilon \ll 1$, it has been shown in [24] that the forward-scattering approximation and the white-noise approximation are both valid, which means that the second-order derivative in z in (3.4) can be neglected and the random potential $\frac{1}{\varepsilon}\mu\big(\boldsymbol{x}, \frac{z}{\varepsilon^2}\big)$ can be replaced by a Gaussian field that is white noise in the z-direction. The mathematical statement is that the random function $\hat{\phi}^\varepsilon(\omega, \boldsymbol{x}, z)$ converges in distribution to the solution $\hat{\phi}(\omega, \boldsymbol{x}, z)$ of the Itô–Schrödinger equation

$$2i\frac{\omega}{c_0}d\hat{\phi}(\omega, \boldsymbol{x}, z) + \Delta_\perp \hat{\phi}(\omega, \boldsymbol{x}, z)dz + \frac{\omega^2}{c_0^2}\hat{\phi}(\omega, \boldsymbol{x}, z) \circ dB(\boldsymbol{x}, z) = 0,$$

where $B(\boldsymbol{x}, z)$ is a Brownian field, that is, a Gaussian process with mean zero and covariance function (2.1). Here the $\circ$ stands for the Stratonovich stochastic integral [24]. We introduce the fundamental solution $\hat{G}(\omega, (\boldsymbol{x}, z), (\boldsymbol{x}_0, z_0))$, which is defined as the solution of the equation in $(\boldsymbol{x}, z)$ (for $z > z_0$):

$$2i\frac{\omega}{c_0}d\hat{G} + \Delta_\perp \hat{G}dz + \frac{\omega^2}{c_0^2}\hat{G} \circ dB(\boldsymbol{x}, z) = 0, \tag{3.5}$$

starting from $\hat{G}(\omega, (\boldsymbol{x}, z = z_0), (\boldsymbol{x}_0, z_0)) = \delta(\boldsymbol{x} - \boldsymbol{x}_0)$. In a homogeneous medium ($B \equiv 0$) the fundamental solution is (for $z > z_0$)

$$\hat{G}_0\big(\omega, (\boldsymbol{x}, z), (\boldsymbol{x}_0, z_0)\big) = \frac{\omega}{2i\pi c_0(z - z_0)}\exp\left(i\frac{\omega|\boldsymbol{x} - \boldsymbol{x}_0|^2}{2c_0(z - z_0)}\right). \tag{3.6}$$

In a random medium, the first two moments of the random fundamental solution have the following expressions.

Proposition 3.1. *The first order-moment of the random fundamental solution exhibits frequency-dependent damping:*

$$\mathbb{E}\big[\hat{G}\big(\omega,(\boldsymbol{x},z),(\boldsymbol{x}_0,z_0)\big)\big]=\hat{G}_0\big(\omega,(\boldsymbol{x},z),(\boldsymbol{x}_0,z_0)\big)\exp\left(-\frac{\gamma_0(\mathbf{0})\omega^2|z-z_0|}{8c_0^2}\right), \tag{3.7}$$

where γ_0 is given by (2.2).

The second order-moment of the random fundamental solution exhibits frequency-dependent spatial decorrelation:

$$\begin{aligned}&\mathbb{E}\big[\hat{G}\big(\omega,(\boldsymbol{x},z),(\boldsymbol{x}_0,z_0)\big)\overline{\hat{G}\big(\omega,(\boldsymbol{x}',z),(\boldsymbol{x}_0,z_0)\big)}\big]\\ &=\hat{G}_0\big(\omega,(\boldsymbol{x},z),(\boldsymbol{x}_0,z_0)\big)\overline{\hat{G}_0\big(\omega,(\boldsymbol{x}',z),(\boldsymbol{x}_0,z_0)\big)}\exp\left(-\frac{\gamma_2(\boldsymbol{x}-\boldsymbol{x}')\omega^2|z-z_0|}{4c_0^2}\right),\end{aligned} \tag{3.8}$$

where

$$\gamma_2(\boldsymbol{x})=\int_0^1\big(\gamma_0(\mathbf{0})-\gamma_0(\boldsymbol{x}s)\big)ds, \tag{3.9}$$

with γ_0 given by (2.2).

These are classical results [27, Chapter 20] once the random paraxial equation has been proved to be correct, as is the case here. The result on the first-order moment shows that any coherent wave imaging method cannot give good images if the range is larger than the scattering mean free path $l_{\rm sca}=8c_0^2/(\gamma_0(\mathbf{0})\omega^2)$, because the coherent wave components will then be exponentially damped. This is the situation we have in mind, and this is the situation in which imaging by migration of cross correlations turns out to be efficient. The results on the second-order moment will be used in the next subsection to analyze the cross correlation of the recorded signals in a quantitative way.

3.3. The cross correlation of the recorded field in the presence of a reflector. We consider again the situation described in the introduction. In the random paraxial scaling regime described above, the scalar field $p^\varepsilon(t,\vec{\boldsymbol{x}};\vec{\boldsymbol{x}}_s)$ corresponding to the emission from an element $\vec{\boldsymbol{x}}_s$ of the surface source array is solution of

$$\frac{1}{c^\varepsilon(\vec{\boldsymbol{x}})^2}\frac{\partial^2 p^\varepsilon}{\partial t^2}-\Delta p^\varepsilon=-\nabla\cdot\vec{\boldsymbol{F}}^\varepsilon(t,\vec{\boldsymbol{x}};\vec{\boldsymbol{x}}_s), \tag{3.10}$$

where the following hold:

(1) The source term is $\vec{\boldsymbol{F}}^\varepsilon(t,\boldsymbol{x},z;\vec{\boldsymbol{x}}_s)=\vec{\boldsymbol{f}}^\varepsilon(t)\delta(z)\delta(\boldsymbol{x}-\boldsymbol{x}_s)$, the pulse is of the form

$$\vec{\boldsymbol{f}}^\varepsilon(t)=f(t/\varepsilon^4)\vec{\boldsymbol{e}}_z,$$

where the support of the Fourier transform of f is bounded away from zero and of rapid decay at infinity, and $\vec{\boldsymbol{e}}_z$ is the unit vector pointing into the z-direction.

(2) The medium is random in the region $z \in (0, L)$:

$$\frac{1}{c^\varepsilon(\vec{\boldsymbol{x}})^2} = \frac{1}{c_0^2}\Big(1 + \varepsilon^3 \mu\Big(\frac{\boldsymbol{x}}{\varepsilon^2}, \frac{z}{\varepsilon^2}\Big)\Big), \qquad \vec{\boldsymbol{x}} \in \mathbb{R}^2 \times (0, L),$$

and homogeneous with background velocity c_0 in the two half-spaces $z \in (-\infty, 0)$ and $z \in (L, \infty)$, except for the reflector as described by (1.9).

We consider the cross correlation of the signals recorded at the receiver array $(\vec{\boldsymbol{x}}_q)_{q=1}^{N_{\rm q}}$ defined by

$$\mathcal{C}^\varepsilon\big(\tau, \vec{\boldsymbol{x}}_q, \vec{\boldsymbol{x}}_{q'}\big) = \int_{\mathbb{R}} \sum_{s=1}^{N_{\rm s}} p^\varepsilon(t, \vec{\boldsymbol{x}}_q; \vec{\boldsymbol{x}}_s) p^\varepsilon(t + \tau, \vec{\boldsymbol{x}}_{q'}; \vec{\boldsymbol{x}}_s) dt. \tag{3.11}$$

Using the Born approximation for the point reflector at $\vec{\boldsymbol{y}}$ in the homogeneous medium below the auxiliary receiver array, we obtain the following proposition proved in [22].

Proposition 3.2. *In the random paraxial wave regime $\varepsilon \to 0$, when there is a point reflector at $\vec{\boldsymbol{y}} = (\boldsymbol{y}, L_y)$ and when the source array covers the whole surface $z = 0$, then the cross correlation of the recorded signals at the receiver array satisfies*

$$\begin{aligned} \mathcal{C}^\varepsilon\left(\frac{2L_y - 2L}{c_0} + \varepsilon^4 s, \vec{\boldsymbol{x}}_q, \vec{\boldsymbol{x}}_{q'}\right) \overset{\varepsilon\to 0}{\longrightarrow} -\frac{i\sigma_{\rm ref}}{4\pi^3 c_0 (L_y - L)^2} \int \omega^3 |\hat{f}(\omega)|^2 \\ \times \exp\left(- i\omega\left(s - \frac{1}{2c_0} \frac{|\boldsymbol{y} - \boldsymbol{x}_q|^2 + |\boldsymbol{y} - \boldsymbol{x}_{q'}|^2}{L_y - L}\right)\right) d\omega \end{aligned} \tag{3.12}$$

in probability.

The convergence in probability of the cross correlation comes from the self-averaging property of the product of two Green's functions when integrated over frequency, which is the case here because the bandwidth of the source (of order ε^{-4}) is much larger than the frequency coherence radius of the Green's function (of order ε^{-2}). The same mechanism ensures the statistical stability of the refocusing during a time-reversal experiment, meaning that the focal spot of the refocused wave depends on the statistical properties of the random medium, but not on the particular realization.

This proposition shows the following:

(1) The cross correlation $\tau \to \mathcal{C}^\varepsilon(\tau, \vec{\boldsymbol{x}}_q, \vec{\boldsymbol{x}}_{q'})$ has a peak at time lag τ equal to

$$\tau_{\boldsymbol{x}_q, \boldsymbol{x}_{q'}} = \frac{2L_y - 2L}{c_0} + \frac{\varepsilon^4}{2c_0} \frac{|\boldsymbol{y} - \boldsymbol{x}_q|^2 + |\boldsymbol{y} - \boldsymbol{x}_{q'}|^2}{L_y - L},$$

since

$$\mathcal{C}^\varepsilon\big(\tau_{\boldsymbol{x}_q, \boldsymbol{x}_{q'}} + \varepsilon^4 s, \vec{\boldsymbol{x}}_q, \vec{\boldsymbol{x}}_{q'}\big) \overset{\varepsilon\to 0}{\longrightarrow} -\frac{i\sigma_{\rm ref}}{4\pi^3 c_0 (L_y - L)^2} \int \omega^3 |\hat{f}(\omega)|^2 e^{-i\omega s} d\omega$$

has a peak centered at $s = 0$. The time lag $\tau_{\boldsymbol{x}_q, \boldsymbol{x}_{q'}}$ is the sum of travel times from $\vec{\boldsymbol{x}}_q$ to $\vec{\boldsymbol{y}}$ and

from $\vec{\boldsymbol{y}}$ to $\vec{\boldsymbol{x}}_{q'}$ in the paraxial approximation:

$$\begin{aligned}\frac{|\vec{\boldsymbol{x}}_q-\vec{\boldsymbol{y}}|}{c_0}+\frac{|\vec{\boldsymbol{y}}-\vec{\boldsymbol{x}}_{q'}|}{c_0}&=\frac{1}{c_0}\sqrt{(L_y-L)^2+\varepsilon^4|\boldsymbol{y}-\boldsymbol{x}_q|^2}+\frac{1}{c_0}\sqrt{(L_y-L)^2+\varepsilon^4|\boldsymbol{y}-\boldsymbol{x}_{q'}|^2}\\&=\frac{2L_y-2L}{c_0}+\frac{\varepsilon^4}{2c_0}\frac{|\boldsymbol{y}-\boldsymbol{x}_q|^2+|\boldsymbol{y}-\boldsymbol{x}_{q'}|^2}{L_y-L}+O(\varepsilon^8)\\&=\tau_{\boldsymbol{x}_q,\boldsymbol{x}_{q'}}+O(\varepsilon^8).\end{aligned}$$

(2) The effect of the random medium has completely disappeared.

The conclusion is therefore that Kirchhoff migration with cross correlations of the receiver array produces images as if the medium were homogeneous and the receiver array were active.

When the source array has a finite aperture, with the source array diameter equal to b, then an important quantity is the effective source array diameter $b_{\rm eff}$ defined by (2.3). The effective source array diameter can be interpreted as that seen from the receiver array through the random medium. It is increased by wave scattering in the random medium. As we will see in the next section, this increase in turn enhances the resolution of the imaging function.

More precisely, the following proposition shows that only the receivers that are within the cone determined by the effective source array diameter contribute to the cross correlation. As a result, the cross correlation is the same as in the case of a source array with full aperture provided that the effective array diameter is larger than a certain threshold value. In the homogeneous case, this requires that the source array diameter must be larger than the threshold value. In the random medium, the source array does not need to be large; only the effective source array diameter needs to be larger than the threshold value, which can be achieved because of the second term in (2.3) which is due to scattering.

Proposition 3.3. *We consider the random paraxial wave regime $\varepsilon\to 0$ when there is a point reflector at $\vec{\boldsymbol{y}}=(\boldsymbol{y},L_y)$ and when the source array covers a domain of radius b at the surface $z=0$. If the effective source array diameter is large enough in the sense that the effective Fresnel number $\frac{b_{\rm eff}^2}{\lambda_0 L}>\frac{L_y}{L_y-L}$, where $\lambda_0=2\pi c_0/\omega_0$ is the carrier wavelength, then the cross correlation of the recorded signals at the receiver array satisfies*

$$\begin{aligned}\mathcal{C}^\varepsilon\Big(\frac{2L_y-2L}{c_0}+\varepsilon^4 s,\vec{\boldsymbol{x}}_q,\vec{\boldsymbol{x}}_{q'}\Big)\stackrel{\varepsilon\to 0}{\longrightarrow}-\frac{i\sigma_{\rm ref}}{4\pi^3 c_0(L_y-L)^2}\int\omega^3|\hat f(\omega)|^2\psi_{\rm eff}(\boldsymbol{x}_q,\boldsymbol{y})\\\times\exp\left(-i\omega\left(s-\frac{1}{2c_0}\frac{|\boldsymbol{y}-\boldsymbol{x}_q|^2+|\boldsymbol{y}-\boldsymbol{x}_{q'}|^2}{L_y-L}\right)\right)d\omega\end{aligned}\tag{3.13}$$

in probability, where

$$\psi_{\rm eff}(\boldsymbol{x}_q,\boldsymbol{y})=\frac{b^2}{b_{\rm eff}^2}\exp\left(-\frac{|\boldsymbol{x}_q-\boldsymbol{y}L/L_y|^2}{a_{\rm eff}^2}\right),\tag{3.14}$$

with $a_{\rm eff}$ and $b_{\rm eff}$ given by (2.3)–(2.4).

In order to get an explicit closed-form expression for the effective truncation function $\psi_{\rm eff}$, we have assumed that the source array is dense (i.e., the distance between the sensors is smaller than or equal to half a central wavelength) and that the source density (or cut-off profile) at the surface $z=0$ is described by the function

$$\psi_{\rm s}(\boldsymbol{x}_s)=\exp(-|\boldsymbol{x}_s|^2/b^2),\tag{3.15}$$

that is, a Gaussian profile with radius b. The previous result is qualitatively true for an arbitrary form of the function $\psi_{\rm s}$, but then the effective truncation function has no closed-form expression.

The finite aperture of the source array limits the angular diversity of the illumination, and as a result only a portion of the receiver array contributes to the cross correlation as characterized by the effective truncation function $\psi_{\rm eff}(\boldsymbol{x}_q, \boldsymbol{y})$. In a homogeneous medium (Figure 3, left) the effective truncation function has a clear geometric interpretation: only the receivers localized along rays going from the sources to the reflector can contribute. In a random medium, the angular diversity of the illumination is enhanced by scattering, and the effective truncation function is characterized by the effective source array diameter $b_{\rm eff}$ that depends on the source array diameter b and on the angular diversity enhancement induced by scattering (see (2.3)). Equation (3.14) shows that, in terms of the effective receiver array diameter $a_{\rm eff}$ defined by (2.4), we have the following:

- If $a_{\rm eff} > a$ so that $|\boldsymbol{x}_q - \boldsymbol{y}L/L_y| < a_{\rm eff}$ for all $\boldsymbol{x}_q$ in the receiver array, then the effective truncation function $\psi_{\rm eff}$ plays no role, and we obtain the same result as in the case of a source array with full, infinite aperture. The Kirchhoff migration function takes the form of (3.22) in this case.
- If $a_{\rm eff} < a$, then the effective truncation function $\psi_{\rm eff}$ does play a role, and we obtain a result that is different from the case of a source array with full aperture. The Kirchhoff migration function takes the form of (3.24) in this case.
- In both cases, scattering is helpful, as it increases the angular diversity and reduces the impact of the effective truncation function $\psi_{\rm eff}$.

Proof. We first describe the different wave signals that can be recorded at the surface array or at the receiver array.

(1) The field recorded at the auxiliary receiver array at $\vec{\boldsymbol{x}}_q = (\boldsymbol{x}_q, L)$ around time L/c_0 is the field transmitted through the scattering layer in $z \in (0, L)$:

$$p^\varepsilon\left(\frac{L}{c_0} + \varepsilon^4 s, \vec{\boldsymbol{x}}_q; \vec{\boldsymbol{x}}_s\right) \overset{\varepsilon\to 0}{\longrightarrow} \frac{1}{2\pi}\int_{-\infty}^{\infty} \hat f(\omega) e^{-i\omega s} \hat G\big(\omega, (\boldsymbol{x}_q, L), (\boldsymbol{x}_s, 0)\big) d\omega.$$

(2) Using the Born approximation for the reflector, the field recorded at the auxiliary receiver array at $\vec{\boldsymbol{x}}_{q'} = (\boldsymbol{x}_{q'}, L)$ around time $(2L_y - L)/c_0$ is of the form

$$\begin{aligned} p^\varepsilon\left(\frac{2L_y - L}{c_0} + \varepsilon^4 s, \vec{\boldsymbol{x}}_{q'}; \vec{\boldsymbol{x}}_s\right) \overset{\varepsilon\to 0}{\longrightarrow} \frac{i\sigma_{\rm ref} c_0}{\pi}\int_{-\infty}^{\infty}\int_{\mathbb{R}^2} \omega \hat f(\omega) e^{-i\omega s} \hat G_0\big(\omega, (\boldsymbol{y}, L_y), (\boldsymbol{x}_{q'}, L)\big) \\ \times \hat G_0\big(\omega, (\boldsymbol{y}, L_y), (\boldsymbol{x}, L)\big) \hat G\big(\omega, (\boldsymbol{x}, L), (\boldsymbol{x}_s, 0)\big) d\boldsymbol{x} d\omega. \end{aligned}$$

In the Born approximation there is no other wave component recorded at $\vec{\boldsymbol{x}}_{q'}$ around a time $t_0 \notin \{L/c_0, (2L_y - L)/c_0\}$.

As a consequence, the cross correlation of the signals recorded at the receiver array defined by (3.11) is concentrated around time lag $2(L_y - L)/c_0$, and it is of the form

$$\begin{aligned} \mathcal{C}^\varepsilon\left(\frac{2L_y - 2L}{c_0} + \varepsilon^4 s, \vec{\boldsymbol{x}}_q, \vec{\boldsymbol{x}}_{q'}\right) \overset{\varepsilon\to 0}{\longrightarrow} \frac{i\sigma_{\rm ref} c_0}{\pi}\int_{-\infty}^{\infty}\int_{\mathbb{R}^2}\int_{\mathbb{R}^2} \omega |\hat f(\omega)|^2 e^{-i\omega s} \psi_{\rm s}(\boldsymbol{x}_s) \\ \times \hat G_0\big(\omega, (\boldsymbol{y}, L_y), (\boldsymbol{x}_{q'}, L)\big) \hat G_0\big(\omega, (\boldsymbol{y}, L_y), (\boldsymbol{x}, L)\big) \\ \times \hat G\big(\omega, (\boldsymbol{x}, L), (\boldsymbol{x}_s, 0)\big) \overline{\hat G\big(\omega, (\boldsymbol{x}_q, L), (\boldsymbol{x}_s, 0)\big)} d\boldsymbol{x}_s d\boldsymbol{x} d\omega \end{aligned}$$

when the source array is dense at the surface $z=0$ and is characterized by the density function $\psi_{\rm s}$. Using Proposition 3.1 and the self-averaging property of the product of two fundamental solutions (one of them being complex conjugated) [28, 29, 24], we get

$$\mathcal{C}^\varepsilon\left(\frac{2L_y-2L}{c_0}+\varepsilon^4 s,\vec{\boldsymbol{x}}_q,\vec{\boldsymbol{x}}_{q'}\right)\stackrel{\varepsilon\to 0}{\longrightarrow}\frac{i\sigma_{\rm ref}c_0}{\pi}\int_{-\infty}^{\infty}\int_{\mathbb{R}^2}\int_{\mathbb{R}^2}\omega|\hat f(\omega)|^2e^{-i\omega s}\psi_{\rm s}(\boldsymbol{x}_s)$$
$$\times\hat G_0\big(\omega,(\boldsymbol{y},L_y),(\boldsymbol{x}_{q'},L)\big)\hat G_0\big(\omega,(\boldsymbol{y},L_y),(\boldsymbol{x},L)\big)$$
$$\times\hat G_0\big(\omega,(\boldsymbol{x},L),(\boldsymbol{x}_s,0)\big)\overline{\hat G_0\big(\omega,(\boldsymbol{x}_q,L),(\boldsymbol{x}_s,0)\big)}$$
$$\times\exp\left(-\frac{\omega^2L\gamma_2(\boldsymbol{x}-\boldsymbol{x}_q)}{4c_0^2}\right)d\boldsymbol{x}_s d\boldsymbol{x}d\omega.$$

When the sources cover the surface $z=0$, i.e., when $\psi_{\rm s}\equiv 1$, we see by integrating in $\boldsymbol{x}_s$ and by using the explicit expression (3.6) that we have a Dirac distribution $\delta(\boldsymbol{x}-\boldsymbol{x}_q)$. The exponential damping term then disappears because $\gamma_2(\boldsymbol{0})=0$ (see (3.9)), and we finally obtain (3.12).

When the source array has finite aperture with diameter b at the surface $z=0$ and can be modeled by the density function $\psi_{\rm s}(\boldsymbol{x}_s)=\exp(-|\boldsymbol{x}_s|^2/b^2)$, we get by integrating in $\boldsymbol{x}_s$ and by using the explicit expression (3.6) that

$$\mathcal{C}^\varepsilon\left(\frac{2L_y-2L}{c_0}+\varepsilon^4 s,\vec{\boldsymbol{x}}_q,\vec{\boldsymbol{x}}_{q'}\right)\stackrel{\varepsilon\to 0}{\longrightarrow}\frac{\sigma_{\rm ref}b^2}{8\pi^3c_0^2L^2(L_y-L)}\int\omega^4|\hat f(\omega)|^2e^{-i\omega s}$$
$$\times\hat G_0\big(\omega,(\boldsymbol{y},L_y),(\boldsymbol{x}_{q'},L)\big)\mathcal{G}\big(\omega,(\boldsymbol{y},L_y),(\boldsymbol{x}_q,L)\big)d\omega,\tag{3.16}$$

with

$$\mathcal{G}\big(\omega,(\boldsymbol{y},L_y),(\boldsymbol{x}_q,L)\big)=\int_{\mathbb{R}^2}\exp\left(i\frac{\omega|\boldsymbol{y}-\boldsymbol{x}|^2}{2c_0(L_y-L)}\right)\exp\left(i\frac{\omega}{2c_0L}(|\boldsymbol{x}|^2-|\boldsymbol{x}_q|^2)\right)$$
$$\times\exp\left(-\frac{\omega^2b^2|\boldsymbol{x}-\boldsymbol{x}_q|^2}{4c_0^2L^2}\right)\exp\left(-\frac{\omega^2L\gamma_2(\boldsymbol{x}-\boldsymbol{x}_q)}{4c_0^2}\right)d\boldsymbol{x}.$$

• When there is no scattering or when scattering is weak in the sense that $\gamma_0(\boldsymbol{0})\omega^2L/c_0^2<1$ for ω in the source bandwidth, then we have $\gamma_2(\boldsymbol{x}-\boldsymbol{x}_q)\omega^2L/c_0^2\simeq 0$ and

$$\exp\left(-\frac{\omega^2b^2|\boldsymbol{x}-\boldsymbol{x}_q|^2}{4c_0^2L^2}\right)\exp\left(-\frac{\omega^2L\gamma_2(\boldsymbol{x}-\boldsymbol{x}_q)}{4c_0^2}\right)\simeq\exp\left(-\frac{\omega^2b_{\rm eff}^2|\boldsymbol{x}-\boldsymbol{x}_q|^2}{4c_0^2L^2}\right),$$

with $b_{\rm eff}=b$.

• When scattering is strong so that $\gamma_0(\boldsymbol{0})\omega^2L/c_0^2>1$ for ω in the source bandwidth, then we have

$$\exp\left(-\frac{\omega^2L\gamma_2(\boldsymbol{x}-\boldsymbol{x}_q)}{4c_0^2}\right)\simeq\exp\left(-\frac{\bar\gamma_2\omega^2L}{12c_0^2}|\boldsymbol{x}-\boldsymbol{x}_q|^2\right),$$

where $\bar\gamma_2$ is such that $\gamma_0(\boldsymbol{x})=\gamma_0(\boldsymbol{0})-\bar\gamma_2|\boldsymbol{x}|^2$ for $|\boldsymbol{x}|\ll 1$, so that $\gamma_2(\boldsymbol{x})=\bar\gamma_2|\boldsymbol{x}|^2/3$ for $|\boldsymbol{x}|\ll 1$ (by expanding (3.9)), and

$$\exp\left(-\frac{\omega^2b^2|\boldsymbol{x}-\boldsymbol{x}_q|^2}{4c_0^2L^2}\right)\exp\left(-\frac{\omega^2L\gamma_2(\boldsymbol{x}-\boldsymbol{x}_q)}{4c_0^2}\right)\simeq\exp\left(-\frac{\omega^2b_{\rm eff}^2|\boldsymbol{x}-\boldsymbol{x}_q|^2}{4c_0^2L^2}\right),$$

with $b_{\rm eff}^2 = b^2 + \frac{\bar\gamma_2 L^3}{3}$, as in (2.3).

By integrating in $\boldsymbol{x}$ the integral in the expression of the function $\mathcal{G}$ we obtain

$$\mathcal{G}(\omega,(\boldsymbol{y},L_y),(\boldsymbol{x}_q,L)) = \frac{\pi}{\frac{\omega^2 b_{\rm eff}^2}{4c_0^2L^2} - \frac{i\omega L_y}{2c_0L(L_y-L)}} \exp\left\{ - \frac{\frac{\omega^2}{4c_0^2}\left|\frac{\boldsymbol{x}_q}{L} + \frac{\boldsymbol{x}_q-\boldsymbol{y}}{L_y-L}\right|^2}{\frac{\omega^2 b_{\rm eff}^2}{4c_0^2L^2} - \frac{i\omega L_y}{2c_0L(L_y-L)}} + \frac{i\omega|\boldsymbol{x}_q-\boldsymbol{y}|^2}{2c_0(L_y-L)}\right\}.$$

If $\frac{\omega_0 b_{\rm eff}}{c_0 L} > \frac{L_y}{L_y-L}$, then

$$\mathcal{G}(\omega,(\boldsymbol{y},L_y),(\boldsymbol{x}_q,L)) = \frac{4\pi c_0^2L^2}{\omega^2 b_{\rm eff}^2} \exp\left\{ - \frac{\left|\boldsymbol{x}_q - \frac{L}{L_y}\boldsymbol{y}\right|^2}{a_{\rm eff}^2} + \frac{i\omega|\boldsymbol{x}_q-\boldsymbol{y}|^2}{2c_0(L_y-L)}\right\}.$$

Substituting into (3.16) gives the desired result. ∎

3.4. Kirchhoff migration of cross correlations. The Kirchhoff migration function for the search point $\vec{\boldsymbol{y}}^S$ is

$$\mathcal{I}_{\rm C}^{\varepsilon}(\vec{\boldsymbol{y}}^S) = \frac{1}{N_{\rm q}^2}\sum_{q,q'=1}^{N_{\rm q}} \mathcal{C}^{\varepsilon}\Big(\frac{|\vec{\boldsymbol{x}}_q - \vec{\boldsymbol{y}}^S| + |\vec{\boldsymbol{y}}^S - \vec{\boldsymbol{x}}_{q'}|}{c_0}, \vec{\boldsymbol{x}}_q, \vec{\boldsymbol{x}}_{q'}\Big), \tag{3.17}$$

where $N_{\rm q}$ is the number of receivers at the auxiliary receiver array. The following proposition describes the resolution properties of the imaging function when the source array has full aperture. It was proved in [22].

Proposition 3.4. *If the auxiliary receiver array at altitude L is a dense square array centered at $(\mathbf{0}, L)$ and with sidelength a, if the source array covers the surface $z = 0$, and if we assume additionally hypothesis (3.18):*

$$\begin{aligned} &\textit{The sidelength } a \textit{ is smaller than } L_y - L.\\ &\textit{The bandwidth } B \textit{ of the source pulse is small compared}\\ &\textit{to the central frequency } \omega_0, \end{aligned} \tag{3.18}$$

then, parameterizing the search point around the reflector by

$$\vec{\boldsymbol{y}}^S = \vec{\boldsymbol{y}} + (\varepsilon^2\boldsymbol{\xi}, \varepsilon^4\eta), \tag{3.19}$$

we have

$$\begin{aligned} \mathcal{I}_{\rm C}^{\varepsilon}(\vec{\boldsymbol{y}}^S) \overset{\varepsilon\to 0}{\longrightarrow} &-\frac{i\sigma_{\rm ref}}{4\pi^3 c_0 (L_y-L)^2} \operatorname{sinc}^2\Big(\frac{\pi a\xi_1}{\lambda_0(L_y-L)}\Big)\operatorname{sinc}^2\Big(\frac{\pi a\xi_2}{\lambda_0(L_y-L)}\Big)\\ &\times \int \omega^3 |\hat f(\omega)|^2 \exp\Big(2i\frac{\omega}{c_0}\eta\Big) d\omega. \end{aligned} \tag{3.20}$$

Note that the result is not changed qualitatively if a is of the same order as or larger than $L_y - L$ or if the bandwidth is of the same order as the central frequency, but then the transverse shape is not a sinc^2 anymore, as explained in [22].

This shows that the migration of the cross correlation gives the same result as if we were migrating the array response matrix of the auxiliary receiver array. Indeed, the imaging

function (3.20) is exactly the imaging function that we would obtain if the medium were homogeneous, if the passive receiver array could be used as an active array, and if the response matrix of the array were migrated to the search point $\vec{\boldsymbol{y}}^S$. In particular, the cross-range resolution is $\lambda_0(L-L_y)/a$, and the range resolution is c_0/B.

The following proposition is a new result, and it describes the resolution properties of the imaging function when the source array has finite aperture.

Proposition 3.5. *If the auxiliary receiver array at altitude L is a dense square array centered at $(\mathbf{0}, L)$ and with sidelength a, if the source array has finite aperture with diameter b and density (3.15), and if we assume additionally hypothesis (3.18), then, parameterizing the search point by (3.19), we have*

$$\begin{aligned}\mathcal{I}_{\rm C}^{\varepsilon}(\vec{\boldsymbol{y}}^S) \stackrel{\varepsilon\to 0}{\longrightarrow} & -\frac{i\sigma_{\rm ref}}{4\pi^3 c_0(L_y-L)^2}\mathrm{sinc}\Big(\frac{\pi a\xi_1}{\lambda_0(L_y-L)}\Big)\mathrm{sinc}\Big(\frac{\pi a\xi_2}{\lambda_0(L_y-L)}\Big)\\ & \times\frac{b^2}{a^2 b_{\rm eff}^2}\int_{[-a/2,a/2]^2} d\boldsymbol{x}_q \exp\Big(-\frac{|\boldsymbol{x}_q-\boldsymbol{y}|^2}{a_{\rm eff}^2}+i\frac{\omega_0}{c_0(L_y-L)}\boldsymbol{\xi}\cdot(\boldsymbol{x}_q-\boldsymbol{y})\Big)\\ & \times\int \omega^3|\hat f(\omega)|^2\exp\Big(2i\frac{\omega}{c_0}\eta\Big)d\omega. \end{aligned} \tag{3.21}$$

This shows the following:

1. If the effective source array diameter is large enough so that $|\boldsymbol{x}_q-\boldsymbol{y}|\le a_{\rm eff}$ for all $\boldsymbol{x}_q\in[-a/2,a/2]^2$, then we get the same result (3.20) as in the case of a source array with full aperture:

$$\begin{aligned}\mathcal{I}_{\rm C}^{\varepsilon}(\vec{\boldsymbol{y}}^S) \stackrel{\varepsilon\to 0}{\longrightarrow} & -\frac{i\sigma_{\rm ref}}{4\pi^3 c_0(L_y-L)^2}\mathrm{sinc}^2\Big(\frac{\pi a\xi_1}{\lambda_0(L_y-L)}\Big)\mathrm{sinc}^2\Big(\frac{\pi a\xi_2}{\lambda_0(L_y-L)}\Big)\\ & \times\int \omega^3|\hat f(\omega)|^2\exp\Big(2i\frac{\omega}{c_0}\eta\Big)d\omega. \end{aligned} \tag{3.22}$$

2. If the effective source array diameter $a_{\rm eff}$ is smaller than a, then we get

$$\begin{aligned}\mathcal{I}_{\rm C}^{\varepsilon}(\vec{\boldsymbol{y}}^S) \stackrel{\varepsilon\to 0}{\longrightarrow} & -\frac{i\sigma_{\rm ref} b^2}{4\pi^2 c_0 L^2 a^2}\mathrm{sinc}\Big(\frac{\pi a\xi_1}{\lambda_0(L_y-L)}\Big)\mathrm{sinc}\Big(\frac{\pi a\xi_2}{\lambda_0(L_y-L)}\Big)\exp\Big(-\frac{\pi^2 a_{\rm eff}^2|\boldsymbol{\xi}|^2}{\lambda_0^2(L_y-L)^2}\Big)\\ & \times\int \omega^3|\hat f(\omega)|^2\exp\Big(2i\frac{\omega}{c_0}\eta\Big)d\omega, \end{aligned} \tag{3.23}$$

where $a_{\rm eff}$ is defined by (2.4). Since $a_{\rm eff}$ is smaller than a, this gives, in fact,

$$\begin{aligned}\mathcal{I}_{\rm C}^{\varepsilon}(\vec{\boldsymbol{y}}^S) \stackrel{\varepsilon\to 0}{\longrightarrow} & -\frac{i\sigma_{\rm ref} b^2}{4\pi^2 c_0 L^2 a^2}\mathrm{sinc}\Big(\frac{\pi a\xi_1}{\lambda_0(L_y-L)}\Big)\mathrm{sinc}\Big(\frac{\pi a\xi_2}{\lambda_0(L_y-L)}\Big)\\ & \times\int \omega^3|\hat f(\omega)|^2\exp\Big(2i\frac{\omega}{c_0}\eta\Big)d\omega. \end{aligned} \tag{3.24}$$

Note that the difference from (3.22) is that the sinc functions have no square. This shows that the cross-range resolution is reduced (compared to the case of a source array with full aperture), and the range resolution is not affected.

4. Imaging through a randomly layered medium. In this section we analyze a scaling regime in which scattering is anisotropic and strong. We consider linear acoustic waves propagating in a three-dimensional layered medium and generated by a point source. Motivated by geophysical applications, we take a typical wavelength of the probing pulse to be larger than the correlation length of the medium and smaller than the propagation distance. This is the regime appropriate in exploration geophysics studied, for instance, in [1, 17, 19, 26]. In the analysis we abstract this regime of physical parameters by introducing the dimensionless parameter ε that captures roughly the ordering of the scale ratios:

$$\frac{l_c}{L} \sim \varepsilon^2, \qquad \frac{\lambda}{L} \sim \varepsilon. \tag{4.1}$$

We consider the situation described in the introduction. In the scaling regime described above, the scalar field $p^\varepsilon(t, \vec{\boldsymbol{x}}; \vec{\boldsymbol{x}}_s)$ corresponding to an element $\vec{\boldsymbol{x}}_s$ of the surface source array is the solution of

$$\frac{1}{c^\varepsilon(\vec{\boldsymbol{x}})^2}\frac{\partial^2 p^\varepsilon}{\partial t^2} - \Delta p^\varepsilon = -\nabla \cdot \vec{\boldsymbol{F}}^\varepsilon(t, \vec{\boldsymbol{x}}; \vec{\boldsymbol{x}}_s). \tag{4.2}$$

Here we have the following:

(1) The source term is $\vec{\boldsymbol{F}}^\varepsilon(t, \vec{\boldsymbol{x}}; \vec{\boldsymbol{x}}_s) = \vec{\boldsymbol{f}}^\varepsilon(t)\delta(z)\delta(\boldsymbol{x} - \boldsymbol{x}_s)$, and the pulse is of the form

$$\vec{\boldsymbol{f}}^\varepsilon(t) = \varepsilon \vec{\boldsymbol{f}}\Big(\frac{t}{\varepsilon}\Big), \tag{4.3}$$

where we assume that the support of the Fourier transform of $\vec{\boldsymbol{f}} = (\boldsymbol{f}_{\boldsymbol{x}}, f_z)$ is bounded away from zero and of rapid decay at infinity. The particular scaling of $\vec{\boldsymbol{f}}^\varepsilon$ in (1.7) means that the central wavelength is large compared to the microscopic scale of variation of the random fluctuations of the medium and small compared to the macroscopic scale of variation of the background medium, as in (4.1). The normalizing amplitude factor ε multiplying the source term is not important as the wave equation is linear, but it will make the quantities of interest of order one as $\varepsilon \to 0$, which explains our choice.

(2) The medium is randomly layered in the region $z \in (0, L)$,

$$\frac{1}{c^\varepsilon(\vec{\boldsymbol{x}})^2} = \frac{1}{c_0^2}\Big(1 + \nu\Big(\frac{z}{\varepsilon^2}\Big)\Big), \qquad \vec{\boldsymbol{x}} = (\boldsymbol{x}, z) \in \mathbb{R}^2 \times (0, L), \tag{4.4}$$

and homogeneous in the region $z \in (L, \infty)$,

$$\frac{1}{c^\varepsilon(\vec{\boldsymbol{x}})^2} = \frac{1}{c_0^2}, \qquad \vec{\boldsymbol{x}} = (\boldsymbol{x}, z) \in \mathbb{R}^2 \times (L, \infty).$$

(3) Dirichlet boundary conditions are imposed at the surface $z = 0$:

$$p^\varepsilon(t, (\boldsymbol{x}, z = 0)) = 0, \qquad \boldsymbol{x} \in \mathbb{R}^2.$$

This boundary condition is motivated by geophysical applications, in which the density in the homogeneous half-space $z \le 0$ (the atmosphere) is much smaller than the density in the

medium for $z \geq 0$ (the earth's crust). Since the velocity and pressure are continuous, the pressure in $z < 0$ goes to zero and hence, by continuity, also at $z = 0$. These are the so-called pressure release boundary conditions. It is possible to extend the results to other boundary conditions, such as the transparent or matched boundary condition [22].

In this model the parameters of the medium have random and rapid fluctuations with a typical scale of variation much smaller than the thickness of the inhomogeneous layer. The small dimensionless parameter ε^2 is the ratio between these two scales. The small-scale random fluctuations are described by the random process $\nu(z)$. The process ν is bounded in magnitude by a constant less than one, so that c^ε is a positive quantity. The random process $\nu(z)$ is stationary and has zero mean. It is supposed to have strong mixing properties so that we can use averaging techniques for stochastic differential equations as presented in [17, Chapter 6]. The important quantity from the statistical point of view is the integrated covariance γ of the fluctuations of the random medium defined by (2.6). By the Wiener–Khintchine theorem it is nonnegative as it is the power spectral density evaluated at zero frequency. The integrated covariance γ plays the role of scattering coefficient. It is of the order of the product of the variance of the medium fluctuations times its correlation length. As will become clear in what follows, the statistics of the wave field depend on the random medium via this integrated covariance or power spectral density.

The strategy to analyze the imaging function (1.5) follows the lines of that in section 3. We need, on the one hand, the statistics of the Green's function in the absence of the reflector (subsection 4.1) and, on the other hand, the integral expression of the recorded field in the presence of the reflector in terms of this Green's function, using the Born approximation for the reflector (subsection 4.2). Then it is possible to analyze the cross correlation of the recorded field (subsection 4.3) and the imaging function (1.5) (subsection 4.4).

4.1. Statistics of the Green's function. When there is no reflector, the field is given by

$$p^\varepsilon(t,\vec{\boldsymbol{x}}_q;\vec{\boldsymbol{x}}_s) = -\frac{1}{(2\pi)^3\varepsilon}\int_{\mathbb{R}}\int \mathcal{G}^\varepsilon_{\omega,\kappa} e^{-i\frac{\omega}{\varepsilon}(t-\boldsymbol{\kappa}\cdot(\boldsymbol{x}_q-\boldsymbol{x}_s)-L/c_0(\kappa))}\hat{f}_z(\omega)\omega^2 d\boldsymbol{\kappa}d\omega\,, \tag{4.5}$$

where the integral in $\boldsymbol{\kappa}$ is over the domain $\{\boldsymbol{\kappa}\in\mathbb{R}^2,\ |\boldsymbol{\kappa}|c_0<1\}$ which corresponds to propagative wave modes. The modes, as parameterized by the slowness vector $\boldsymbol{\kappa}$ and the frequency ω, are evanescent if $\kappa > 1/c_0$, where we use the notation $\kappa = |\boldsymbol{\kappa}|$. Here

- $c_0(\kappa)$ is the mode-dependent velocity

$$c_0(\kappa) = \frac{c_0}{\sqrt{1-\kappa^2 c_0^2}}. \tag{4.6}$$

- The random complex coefficient $\mathcal{G}^\varepsilon_{\omega,\kappa}$ is the Fourier-transformed Green's function (for Dirichlet boundary conditions at the surface $z = 0$). The Fourier transform is taken both with respect to time and with respect to the transverse spatial variables. The Green's function can be expressed in terms of the mode-dependent reflection and transmission coefficients $R^\varepsilon_{\omega,\kappa}$ and $T^\varepsilon_{\omega,\kappa}$ of the random section (for matched boundary conditions, that is, transparent boundary conditions) in the following way:

$$\mathcal{G}^\varepsilon_{\omega,\kappa} = \frac{T^\varepsilon_{\omega,\kappa}}{1-R^\varepsilon_{\omega,\kappa}} = \sum_{j=0}^{\infty} T^\varepsilon_{\omega,\kappa}(R^\varepsilon_{\omega,\kappa})^j. \tag{4.7}$$

When the medium is homogeneous, we have $\mathcal{G}^{\varepsilon}_{\omega,\kappa} = 1$ for all ω, κ. When the medium is randomly layered, the statistics of $|\mathcal{G}^{\varepsilon}_{\omega,\kappa}|^2$ were studied in [25]. In particular, it was shown that $\mathbb{E}[|\mathcal{G}^{\varepsilon}_{\omega,\kappa}|^2] \overset{\varepsilon\to 0}{\longrightarrow} 1$, which is the result that is necessary and sufficient to study the cross correlation of the recorded signals for a source array with full aperture. In the case of a source array with finite aperture, the moment of the Green's function at two nearby slownesses is needed. The second-order statistics of the Green's function is described in the following proposition proved in [25, Proposition 5.1].

Proposition 4.1. *The autocovariance function of the Green's function at two nearby slownesses satisfies*

$$\mathbb{E}\big[\mathcal{G}^{\varepsilon}_{\omega,\kappa+\varepsilon\lambda/2}\overline{\mathcal{G}^{\varepsilon}_{\omega,\kappa-\varepsilon\lambda/2}}\big] \overset{\varepsilon\to 0}{\longrightarrow} \int \mathcal{U}(\omega,\kappa,\xi)\exp\big(-i\omega\kappa\lambda\xi\big)d\xi. \tag{4.8}$$

The spectral density $\mathcal{U}(\omega,\kappa,\xi)$ has a probabilistic representation. For a fixed (ω,κ), it is the probability density function of a random variable

$$\mathcal{U}(\omega,\kappa,\xi) = \mathbb{E}\Big[\delta\Big(\xi - 2c_0(\kappa)\int_0^L N_{\omega,\kappa}(z)dz\Big)\Big|N_{\omega,\kappa}(0)=0\Big], \tag{4.9}$$

where $(N_{\omega,\kappa}(z))_{0\le z\le L}$ is a jump Markov process with state space $\mathbb{N}$ and infinitesimal generator

$$\mathcal{L}\phi(N) = \frac{\gamma c_0^2(\kappa)\omega^2}{4c_0^4}\big[(N+1)^2(\phi(N+1)-\phi(N)) + N^2(\phi(N-1)-\phi(N))\big]. \tag{4.10}$$

The result stated in the previous proposition describes completely the autocovariance function of the Green's function, but it is not explicit enough for the forthcoming analysis. Explicit results will be obtained from the following proposition, which is new although it follows from the results obtained in [17, Chapter 9]. It characterizes the transition probabilities of the jump Markov process $(N_{\omega,\kappa}(z))_{0\le z\le L}$ that is used in the probabilistic representation (4.9) of the spectral density $\mathcal{U}$.

Proposition 4.2. *The transition probabilities of the jump Markov process $N_{\omega,\kappa}$ are*

$$\begin{aligned}\mathbb{P}\big(N_{\omega,\kappa}(z_0+z)=n\,\big|\,N_{\omega,\kappa}(z_0)=p\big) &= \exp\Big(-\frac{\gamma c_0^2(\kappa)\omega^2}{16c_0^4}z\Big)\\ &\times\int_0^\infty \exp\Big(-u^2\frac{\gamma c_0^2(\kappa)\omega^2}{4c_0^4}z\Big)Q_{n,p}(u)\frac{2\pi u\sinh(\pi u)}{\cosh^2(\pi u)}du,\end{aligned} \tag{4.11}$$

where

$$Q_{n,p}(u) = P_n(u)P_p(u), \qquad u\in[0,\infty), \quad n,p\in\mathbb{N}, \tag{4.12}$$

and

$$P_n(u) = \sum_{j=0}^n \binom{j}{n}(-1)^j K_j(u), \qquad K_0(u)=1, \qquad K_n(u) = \prod_{j=1}^n \frac{1}{j^2}\Big[u^2+\Big(j-\frac{1}{2}\Big)^2\Big], \tag{4.13}$$

or, equivalently,

$$P_{n+1}(u) = \frac{2n^2+2n+\frac{3}{4}-u^2}{(n+1)^2}P_n(u) - \frac{n^2}{(n+1)^2}P_{n-1}(u), \tag{4.14}$$

$$P_0(u) = 1, \qquad P_1(u) = \frac{3}{4} - u^2. \tag{4.15}$$

The polynomials $P_n(u)$ are orthonormal for the weight function $\frac{2\pi u \sinh(\pi u)}{\cosh^2(\pi u)}\mathbf{1}_{[0,\infty)}(u)$.

4.2. The integral representation of the field. In the presence of a reflector at $\vec{\boldsymbol{y}} = (\boldsymbol{y}, L_y)$, the scalar field at the position $\vec{\boldsymbol{x}}_q = (\boldsymbol{x}_q, L)$ can be decomposed in a primary field and a secondary field:

$$p^\varepsilon(t, \vec{\boldsymbol{x}}_q; \vec{\boldsymbol{x}}_s) = p^\varepsilon_{\rm p}(t, \vec{\boldsymbol{x}}_q; \vec{\boldsymbol{x}}_s) + p^\varepsilon_{\rm s}(t, \vec{\boldsymbol{x}}_q; \vec{\boldsymbol{x}}_s).$$

The primary field $p^\varepsilon_{\rm p}$ is the field obtained in the absence of the reflector given by

$$p^\varepsilon_{\rm p}(t, \vec{\boldsymbol{x}}_q; \vec{\boldsymbol{x}}_s) = -\frac{1}{(2\pi)^3\varepsilon}\int \mathcal{G}^\varepsilon_{\omega,\boldsymbol{\kappa}} e^{-i\frac{\omega}{\varepsilon}(t-\boldsymbol{\kappa}\cdot(\boldsymbol{x}_q-\boldsymbol{x}_s)-L/c_0(\kappa))}\hat{f}_z(\omega)\omega^2 d\omega d\boldsymbol{\kappa}\,. \tag{4.16}$$

The secondary field $p^\varepsilon_{\rm s}$ is the additional contribution due to the reflector localized at $\vec{\boldsymbol{y}} = (\boldsymbol{y}, L_y)$ and given by

$$p^\varepsilon_{\rm s}(t, \vec{\boldsymbol{x}}_q; \vec{\boldsymbol{x}}_s) = \frac{i\sigma_{\rm ref}}{2(2\pi)^5\varepsilon^2}\int \Big(\frac{1}{c_0(\kappa')} - c_0(\kappa)\boldsymbol{\kappa}\cdot\boldsymbol{\kappa}'\Big)\hat{f}_z(\omega)\omega^5\mathcal{G}^\varepsilon_{\omega,\boldsymbol{\kappa}'} \times e^{i\frac{\omega}{\varepsilon}\phi(\boldsymbol{\kappa},\boldsymbol{\kappa}')}d\omega d\boldsymbol{\kappa} d\boldsymbol{\kappa}'\,, \tag{4.17}$$

where the rapidly varying phase is

$$\phi(\boldsymbol{\kappa}, \boldsymbol{\kappa}') = -t + \boldsymbol{\kappa}\cdot(\boldsymbol{x}_q - \boldsymbol{y}) + \frac{L_y - L}{c_0(\kappa)} + \boldsymbol{\kappa}'\cdot(\boldsymbol{y} - \boldsymbol{x}_s) + \frac{L_y}{c_0(\kappa')}\,. \tag{4.18}$$

This expression has been obtained using the Born approximation for the reflector.

4.3. The cross correlation of the recorded field in the presence of a reflector. The cross correlation $\mathcal{C}^\varepsilon$ of the signals recorded at the receiver array is defined by (3.11). If the source array is dense with density (or cut-off profile) $\psi_{\rm s}(\boldsymbol{x}_s)$, then the cross correlation has the form

$$\mathcal{C}^\varepsilon(\tau, \vec{\boldsymbol{x}}_q, \vec{\boldsymbol{x}}_{q'}) = \varepsilon^{-2}\int_{\mathbb{R}^2} d\boldsymbol{x}_s \psi_{\rm s}(\boldsymbol{x}_s)\int dt p^\varepsilon(t, \vec{\boldsymbol{x}}_q; \vec{\boldsymbol{x}}_s)p^\varepsilon(t+\tau, \vec{\boldsymbol{x}}_{q'}; \vec{\boldsymbol{x}}_s). \tag{4.19}$$

In the presence of a reflector at $\vec{\boldsymbol{y}}$, it can be written as the sum

$$\mathcal{C}^\varepsilon(\tau, \vec{\boldsymbol{x}}_q, \vec{\boldsymbol{x}}_{q'}) = \mathcal{C}^\varepsilon_{\rm pp}(\tau, \vec{\boldsymbol{x}}_q, \vec{\boldsymbol{x}}_{q'}) + \mathcal{C}^\varepsilon_{\rm ps}(\tau, \vec{\boldsymbol{x}}_q, \vec{\boldsymbol{x}}_{q'}) + \mathcal{C}^\varepsilon_{\rm sp}(\tau, \vec{\boldsymbol{x}}_q, \vec{\boldsymbol{x}}_{q'}). \tag{4.20}$$

Here $\mathcal{C}^\varepsilon_{\rm pp}$ is the cross correlation of the primary field (4.16) at $\vec{\boldsymbol{x}}_q = (\boldsymbol{x}_q, L)$ with the primary field at $\vec{\boldsymbol{x}}_{q'} = (\boldsymbol{x}_{q'}, L)$,

$$\mathcal{C}^\varepsilon_{\rm pp}(\tau, \vec{\boldsymbol{x}}_q, \vec{\boldsymbol{x}}_{q'}) = \varepsilon^{-2}\int_{\mathbb{R}^2} d\boldsymbol{x}_s \psi_{\rm s}(\boldsymbol{x}_s)\int dt p^\varepsilon_{\rm p}(t, \vec{\boldsymbol{x}}_q; \vec{\boldsymbol{x}}_s)p^\varepsilon_{\rm p}(t+\tau, \vec{\boldsymbol{x}}_{q'}; \vec{\boldsymbol{x}}_s), \tag{4.21}$$

$\mathcal{C}^{\varepsilon}_{\rm ps}$ is the cross correlation of the primary field (4.16) at $\vec{\boldsymbol{x}}_q$ with the secondary field (4.17) at $\vec{\boldsymbol{x}}_{q'}$,

$$\mathcal{C}^{\varepsilon}_{\rm ps}(\tau,\vec{\boldsymbol{x}}_q,\vec{\boldsymbol{x}}_{q'}) = \varepsilon^{-2}\int_{\mathbb{R}^2} d\boldsymbol{x}_s\psi_{\rm s}(\boldsymbol{x}_s)\int dt p^{\varepsilon}_{\rm p}(t,\vec{\boldsymbol{x}}_q;\vec{\boldsymbol{x}}_s)p^{\varepsilon}_{\rm s}(t+\tau,\vec{\boldsymbol{x}}_{q'};\vec{\boldsymbol{x}}_s), \tag{4.22}$$

and $\mathcal{C}^{\varepsilon}_{\rm sp}$ is the cross correlation of the secondary field (4.17) at $\vec{\boldsymbol{x}}_q$ with the primary field (4.16) at $\vec{\boldsymbol{x}}_{q'}$,

$$\mathcal{C}^{\varepsilon}_{\rm sp}(\tau,\vec{\boldsymbol{x}}_q,\vec{\boldsymbol{x}}_{q'}) = \varepsilon^{-2}\int_{\mathbb{R}^2} d\boldsymbol{x}_s\psi_{\rm s}(\boldsymbol{x}_s)\int dt p^{\varepsilon}_{\rm s}(t,\vec{\boldsymbol{x}}_q;\vec{\boldsymbol{x}}_s)p^{\varepsilon}_{\rm p}(t+\tau,\vec{\boldsymbol{x}}_{q'};\vec{\boldsymbol{x}}_s). \tag{4.23}$$

The following proposition gives a closed-form expression of the cross correlation in the asymptotic regime $\varepsilon\to 0$.

Proposition 4.3. *For $\vec{\boldsymbol{y}} = (\boldsymbol{y}, L_y)$ and $\vec{\boldsymbol{x}}_q = (\boldsymbol{x}_q, L)$, the ps-secondary cross correlation (4.22) centered at $\tau = [|\vec{\boldsymbol{y}}-\vec{\boldsymbol{x}}_q| + |\vec{\boldsymbol{x}}_{q'}-\vec{\boldsymbol{y}}|]/c_0$ has the asymptotic form*

$$\begin{aligned}&\mathcal{C}^{\varepsilon}_{\rm ps}\Big(\frac{|\vec{\boldsymbol{y}}-\vec{\boldsymbol{x}}_q| + |\vec{\boldsymbol{x}}_{q'}-\vec{\boldsymbol{y}}|}{c_0} + \varepsilon s, \vec{\boldsymbol{x}}_q, \vec{\boldsymbol{x}}_{q'}\Big)\\ &\xrightarrow{\varepsilon\to 0} \frac{i\sigma_{\rm ref}}{2(2\pi)^3 c_0^3}\frac{|L_y-L|\,(\vec{\boldsymbol{y}}-\vec{\boldsymbol{x}}_q)\cdot(\vec{\boldsymbol{x}}_{q'}-\vec{\boldsymbol{y}})}{|\vec{\boldsymbol{y}}-\vec{\boldsymbol{x}}_q|^3\,|\vec{\boldsymbol{x}}_{q'}-\vec{\boldsymbol{y}}|^2}\\ &\qquad\times\int \Psi_{\rm eff}\big(\omega,\vec{\boldsymbol{x}}_q,\vec{\boldsymbol{y}}\big)|\hat{f}_z(\omega)|^2\omega^3\exp\big(i\omega s\big)d\omega\end{aligned}$$

in probability, where

$$\begin{aligned}\Psi_{\rm eff}\big(\omega,\vec{\boldsymbol{x}}_q,\vec{\boldsymbol{y}}\big) = \int_{\mathbb{R}}\psi_{\rm s}\Big(\boldsymbol{x}_q - (\boldsymbol{y}-\boldsymbol{x}_q)\Big(\frac{\xi}{c_0|\vec{\boldsymbol{y}}-\vec{\boldsymbol{x}}_q|}+\frac{L}{L_y-L}\Big)\Big)\\ \times\mathcal{U}\Big(\omega,\frac{|\boldsymbol{y}-\boldsymbol{x}_q|}{c_0|\vec{\boldsymbol{y}}-\vec{\boldsymbol{x}}_q|},\xi\Big)d\xi.\end{aligned} \tag{4.24}$$

The ps-secondary cross correlation (4.22) is negligible elsewhere.

As in the random paraxial case, the convergence in probability of the cross correlation comes from the self-averaging property of the product of two Green's functions when integrated over frequency.

Let us first consider the case in which there is no scattering. Then the spectral density is

$$\mathcal{U}(\omega,\kappa,\xi) = \delta(\xi),$$

and we have

$$\begin{aligned}&\mathcal{C}^{\varepsilon}_{\rm ps}\Big(\frac{|\vec{\boldsymbol{y}}-\vec{\boldsymbol{x}}_q| + |\vec{\boldsymbol{x}}_{q'}-\vec{\boldsymbol{y}}|}{c_0} + \varepsilon s, \vec{\boldsymbol{x}}_q, \vec{\boldsymbol{x}}_{q'}\Big)\\ &\xrightarrow{\varepsilon\to 0} \frac{i\sigma_{\rm ref}}{2(2\pi)^3 c_0^3}\frac{|L_y-L|\,(\vec{\boldsymbol{y}}-\vec{\boldsymbol{x}}_q)\cdot(\vec{\boldsymbol{x}}_{q'}-\vec{\boldsymbol{y}})}{|\vec{\boldsymbol{y}}-\vec{\boldsymbol{x}}_q|^3\,|\vec{\boldsymbol{x}}_{q'}-\vec{\boldsymbol{y}}|^2}\psi_{\rm s}\big(\boldsymbol{X}(\boldsymbol{x}_q)\big)\int|\hat{f}_z(\omega)|^2\omega^3\exp\big(i\omega s\big)d\omega,\end{aligned}$$

where

$$\boldsymbol{X}(\boldsymbol{x}_q) = \boldsymbol{x}_q - (\boldsymbol{y}-\boldsymbol{x}_q)\frac{L}{L_y-L}$$

is the intersection of the ray going through $\vec{\boldsymbol{y}}$ and $\vec{\boldsymbol{x}}_q$ with the surface $z=0$. The geometric interpretation is clear: in absence of scattering, the receiver at $\vec{\boldsymbol{x}}_q$ can contribute to the cross correlation only if there is a ray going from the source to the target through it. If $\psi_{\rm s}(\boldsymbol{x}) = \mathbf{1}_{[-b/2,b/2]^2}(\boldsymbol{x})$ and $\boldsymbol{y}=\mathbf{0}$, then we find that $\psi_{\rm s}(\boldsymbol{X}(\boldsymbol{x}_q)) = \mathbf{1}_{[-a_{\rm eff}/2,a_{\rm eff}/2]^2}(\boldsymbol{x}_q)$ with $a_{\rm eff} = (L_y-L)b/L_y$ (see Figure 4, left). If $a_{\rm eff} < a$, then this means that the receiver array cannot be used to its maximal spatial capacity because of limited angular source illumination.

Let us consider the case of a randomly layered medium. In the strongly scattering regime the effective truncation function $\Psi_{\rm eff}$ defined by (4.24) takes a simple form.

Lemma 4.4. *When there is strong scattering in the sense that $L \gg L_{\rm loc}$ and when $\psi_{\rm s}$ is compactly supported in some bounded domain with diameter $b \ll \sqrt{LL_{\rm loc}}$, then*

$$\Psi_{\rm eff}\big(\omega,(\boldsymbol{x}_q,L),(\boldsymbol{y},L_y)\big) \simeq C_{\psi_{\rm s}}\Big(\frac{L_{\rm loc}}{L}\Big)^{3/2}\exp\Big(-\frac{L}{4L_{\rm loc}}\frac{\omega^2}{\omega_0^2}-\frac{L}{4L_{\rm loc}}\frac{|\boldsymbol{y}-\boldsymbol{x}_q|^2}{(L_y-L)^2}\Big)$$

for some constant $C_{\psi_{\rm s}}$ that depends on the source density $\psi_{\rm s}$.

Note that the effective truncation function can also be written as

$$\Psi_{\rm eff}\big(\omega,(\boldsymbol{x}_q,L),(\boldsymbol{y},L_y)\big) \simeq C_{\psi_{\rm s}}\Big(\frac{L_{\rm loc}}{L}\Big)^{3/2}\exp\Big(-\frac{L}{4L_{\rm loc}}\frac{\omega^2}{\omega_0^2}-\frac{|\boldsymbol{y}-\boldsymbol{x}_q|^2}{a_{\rm eff}^2}\Big),$$

in terms of the effective receiver array diameter $a_{\rm eff}$ defined by (2.7)–(2.8). The effective truncation function determines which receivers contribute to the imaging function of the reflector located at $(\boldsymbol{y},L_y)$.

Proof. We use the probabilistic representation of $\mathcal{U}$ given in Proposition 4.1. We note first that, since $N_{\omega,\kappa}(z)$ takes nonnegative values, the function $\xi \to \mathcal{U}(\omega,\kappa,\xi)$ is supported in $[0,\infty)$. From Propositions 4.1–4.2, when $z/L_{\omega,\kappa} \gg 1$ and $n,p=O(1)$, we have

$$\mathbb{P}\big(N_{\omega,\kappa}(z_0+z)=n \,\big|\, N_{\omega,\kappa}(z_0)=p\big) = \exp\Big(-\frac{z}{4L_{\omega,\kappa}}\Big)\frac{\pi^{5/2}Q_{n,p}(0)}{2(z/L_{\omega,\kappa})^{3/2}}\big(1+o(1)\big), \tag{4.25}$$

where

$$L_{\omega,\kappa} = L_{\rm loc}\frac{c_0^2}{c_0(\kappa)^2}\frac{\omega_0^2}{\omega^2}.$$

As a consequence, for any M, there exists C_M such that

$$\mathbb{P}\Big(\int_0^L N_{\omega,\kappa}(z)dz \le M\Big) = \exp\Big(-\frac{L}{4L_{\omega,\kappa}}\Big)\frac{C_M}{(L/L_{\omega,\kappa})^{3/2}}\big(1+o(1)\big) \tag{4.26}$$

when $L/L_{\omega,\kappa} \gg 1$. With $\kappa = |\boldsymbol{y}-\boldsymbol{x}_q|/(|\vec{\boldsymbol{y}}-\vec{\boldsymbol{x}}_q|c_0)$, we have

$$\frac{1}{L_{\omega,\kappa}} = \frac{1}{L_{\rm loc}}\frac{\omega^2}{\omega_0^2}\Big(1+\frac{|\boldsymbol{y}-\boldsymbol{x}_q|^2}{(L_y-L)^2}\Big),$$

which gives the desired result. ∎

4.4. Kirchhoff migration of cross correlations. The Kirchhoff migration function for the search point $\vec{\boldsymbol{y}}^S$ is

$$\mathcal{I}_{\mathrm{C}}^{\varepsilon}(\vec{\boldsymbol{y}}^S) = \frac{1}{N_{\mathrm{q}}^2} \sum_{q,q'=1}^{N_{\mathrm{q}}} \mathcal{C}^{\varepsilon}\Big(\frac{|\vec{\boldsymbol{x}}_q - \vec{\boldsymbol{y}}^S| + |\vec{\boldsymbol{y}}^S - \vec{\boldsymbol{x}}_{q'}|}{c_0}, \vec{\boldsymbol{x}}_q, \vec{\boldsymbol{x}}_{q'}\Big), \tag{4.27}$$

where N_{q} is the number of receivers at the auxiliary receiver array.

When the source array has full aperture, we find that the Kirchhoff migration function gives an image that does not depend on scattering and is the same one as if the medium were homogeneous [22].

Proposition 4.5. *If the auxiliary receiver array at altitude L is a dense square array with sidelength a, and if the source array covers the surface $z = 0$, then, parameterizing the search point by*

$$\vec{\boldsymbol{y}}^S = \vec{\boldsymbol{y}} + \varepsilon(\boldsymbol{\xi}, \eta), \tag{4.28}$$

we have

$$\begin{aligned}\mathcal{I}_{\mathrm{C}}^{\varepsilon}(\vec{\boldsymbol{y}}^S) \overset{\varepsilon\to 0}{\longrightarrow} & \frac{i\sigma_{\mathrm{ref}}}{2(2\pi)^3 c_0^3 (L_y - L)^2} \mathrm{sinc}^2\Big(\frac{\pi a \xi_1}{\lambda_0(L_y - L)}\Big) \mathrm{sinc}^2\Big(\frac{\pi a \xi_2}{\lambda_0(L_y - L)}\Big) \\ & \times \int \omega^3 |\hat{f}_z(\omega)|^2 \exp\Big(2i\frac{\omega}{c_0}\Big(\eta - \frac{\boldsymbol{\xi}\cdot\boldsymbol{y}}{L_y - L}\Big)\Big) d\omega.\end{aligned} \tag{4.29}$$

When the source array has finite aperture, Kirchhoff migration does not give the same image in the presence and in the absence of random scattering. In the randomly layered regime addressed in this section, random scattering reduces the angular diversity of the illumination of the region of interest above the random medium. As a result the image resolution is reduced, as shown by the following proposition.

Proposition 4.6. *If the auxiliary receiver array at altitude L is a dense square array centered at $(\boldsymbol{x}_{\mathrm{A}}, L)$ and with sidelength a if the source array has finite diameter b at the surface $z = 0$, and if we parameterize the search point by (4.28), then we have*

$$\begin{aligned}\mathcal{I}_{\mathrm{C}}^{\varepsilon}(\vec{\boldsymbol{y}}^S) \overset{\varepsilon\to 0}{\longrightarrow} & \frac{i\sigma_{\mathrm{ref}}}{2(2\pi)^3 c_0^3 (L_y - L)^2} \mathrm{sinc}\Big(\frac{\pi a \xi_1}{\lambda_0(L_y - L)}\Big) \mathrm{sinc}\Big(\frac{\pi a \xi_2}{\lambda_0(L_y - L)}\Big) \\ & \times \int d\omega \omega^3 |\hat{f}_z(\omega)|^2 \exp\Big(2i\frac{\omega}{c_0}\Big(\eta - \frac{\boldsymbol{\xi}\cdot\boldsymbol{y}}{L_y - L}\Big)\Big) \\ & \times \frac{1}{a^2} \iint_{[-a/2,a/2]^2} \Psi_{\mathrm{eff}}\big(\omega, (\boldsymbol{x}_q, -L), (\boldsymbol{y}, -L_y)\big) \exp\Big(i\frac{\omega}{c_0}\frac{\boldsymbol{\xi}\cdot\boldsymbol{x}_q}{L_y - L}\Big) d\boldsymbol{x}_q\end{aligned} \tag{4.30}$$

in probability, where Ψ_{eff} is defined by (4.24).

Assume $\boldsymbol{y} = \boldsymbol{0}$ for simplicity.

If scattering is weak ($L \ll L_{\mathrm{loc}}$), then

$$\begin{aligned}\mathcal{I}_{\mathrm{C}}^{\varepsilon}(\vec{\boldsymbol{y}}^S) \overset{\varepsilon\to 0}{\longrightarrow} & \frac{i\sigma_{\mathrm{ref}} a_{\mathrm{eff}}^2}{2(2\pi)^3 c_0^3 (L_y - L)^2 a^2} \mathrm{sinc}\Big(\frac{\pi a \xi_1}{\lambda_0(L_y - L)}\Big) \mathrm{sinc}\Big(\frac{\pi a \xi_2}{\lambda_0(L_y - L)}\Big) \\ & \times \mathrm{sinc}\Big(\frac{\pi a_{\mathrm{eff}} \xi_1}{\lambda_0(L_y - L)}\Big) \mathrm{sinc}\Big(\frac{\pi a_{\mathrm{eff}} \xi_2}{\lambda_0(L_y - L)}\Big) \int \omega^3 |\hat{f}_z(\omega)|^2 \exp\Big(2i\frac{\omega}{c_0}\eta\Big) d\omega,\end{aligned} \tag{4.31}$$

with $a_{\rm eff} = \min\big((L_y - L)b/L_y, a\big)$.

If scattering is strong ($L \gg L_{\rm loc}$)*, then*

$$\mathcal{I}_{\rm C}^{\varepsilon}(\vec{\boldsymbol{y}}^S) \stackrel{\varepsilon\to 0}{\longrightarrow} \frac{i\sigma_{\rm ref} L_{\rm loc}}{(2\pi)^2 c_0^3 L a^2} \mathrm{sinc}\Big(\frac{\pi a \xi_1}{\lambda_0(L_y - L)}\Big)\mathrm{sinc}\Big(\frac{\pi a \xi_2}{\lambda_0(L_y - L)}\Big) \exp\Big(-\frac{\pi^2 L_{\rm loc}|\boldsymbol{\xi}|^2}{L\lambda_0^2}\Big)$$
$$\times \int \omega^3 |\hat{f}_z(\omega)|^2 \exp\Big(-\frac{L\omega^2}{4L_{\rm loc}\omega_0^2}\Big) \exp\Big(2i\frac{\omega}{c_0}\eta\Big) d\omega. \tag{4.32}$$

Note that, when $L \gg L_{\rm loc}$, the Gaussian profile is much broader than the sinc profile in (4.32) and can therefore be neglected.

If, in particular,

$$\hat{f}(\omega) = \exp\Big(-\frac{(\omega - \omega_0)^2}{2B^2}\Big),$$

then, in the weak scattering regime ($L \ll L_{\rm loc}$) we have

$$\mathcal{I}_{\rm C}^{\varepsilon}(\vec{\boldsymbol{y}}^S) \stackrel{\varepsilon\to 0}{\longrightarrow} \frac{i\omega_0^3\sqrt{\pi} B \sigma_{\rm ref} a_{\rm eff}^2}{2(2\pi)^3 c_0^3 (L_y - L)^2 a^2} \mathrm{sinc}\Big(\frac{\pi a \xi_1}{\lambda_0(L_y - L)}\Big)\mathrm{sinc}\Big(\frac{\pi a \xi_2}{\lambda_0(L_y - L)}\Big)$$
$$\times \mathrm{sinc}\Big(\frac{\pi a_{\rm eff} \xi_1}{\lambda_0(L_y - L)}\Big)\mathrm{sinc}\Big(\frac{\pi a_{\rm eff} \xi_2}{\lambda_0(L_y - L)}\Big) \exp\Big(-\frac{B^2\eta^2}{c_0^2}\Big), \tag{4.33}$$

and in the strong scattering regime ($L \gg L_{\rm loc}$) we have

$$\mathcal{I}_{\rm C}^{\varepsilon}(\vec{\boldsymbol{y}}^S) \stackrel{\varepsilon\to 0}{\longrightarrow} \frac{i\omega_0^3\sqrt{\pi} B \sigma_{\rm ref} L_{\rm loc}}{(2\pi)^2 c_0^3 L a^2 \sqrt{1 + \frac{B^2 L}{4\omega_0^2 L_{\rm loc}}}} \exp\Big(-\frac{L}{4L_{\rm loc}\big(1 + \frac{B^2 L}{4\omega_0^2 L_{\rm loc}}\big)}\Big)$$
$$\times \mathrm{sinc}\Big(\frac{\pi a \xi_1}{\lambda_0(L_y - L)}\Big)\mathrm{sinc}\Big(\frac{\pi a \xi_2}{\lambda_0(L_y - L)}\Big)$$
$$\times \exp\Big(-\frac{B^2\eta^2}{c_0^2\big(1 + \frac{B^2 L}{4\omega_0^2 L_{\rm loc}}\big)}\Big) \exp\Big(-i\frac{B^2 L\eta}{2\omega_0 L_{\rm loc} c_0 \big(1 + \frac{B^2 L}{4\omega_0^2 L_{\rm loc}}\big)}\Big). \tag{4.34}$$

We can see that both the cross-range resolution and the range resolution have been reduced by scattering.

The reduction in cross-range resolution comes from the reduction in the effective illumination cone discussed above.

The reduction in range resolution comes from the fact that the high-frequency components are more sensitive to scattering by thin random layers, and therefore the effective spectrum used in the imaging function is reduced compared to the original source spectrum.

Acknowledgment. J. Garnier and G. Papanicolaou thank the Institut des Hautes Études Scientifiques (IHÉS) for its hospitality while this work was completed.

REFERENCES

[1] M. Asch, W. Kohler, G. Papanicolaou, M. Postel, and B. White, *Frequency content of randomly scattered signals*, SIAM Rev., 33 (1991), pp. 519–625.

[2] A. Bakulin and R. Calvert, *The virtual source method: Theory and case study*, Geophysics, 71 (2006), pp. SI139–SI150.

[3] B. Biondi, *3D Seismic Imaging*, Society of Exploration Geophysics, Tulsa, OK, 2006.

[4] N. Bleistein, J. K. Cohen, and J. W. Stockwell, *Mathematics of Multidimensional Seismic Imaging, Migration, and Inversion*, Springer, New York, 2001.

[5] P. Blomgren, G. Papanicolaou, and H. Zhao, *Super-resolution in time-reversal acoustics*, J. Acoust. Soc. Amer., 111 (2002), pp. 230–248.

[6] L. Borcea, J. Garnier, G. Papanicolaou, and C. Tsogka, *Coherent interferometric imaging, time gating, and beamforming*, Inverse Problems, 27 (2011), 065008.

[7] L. Borcea, J. Garnier, G. Papanicolaou, and C. Tsogka, *Enhanced statistical stability in coherent interferometric imaging*, Inverse Problems, 27 (2011), 085004.

[8] L. Borcea, F. González del Cueto, G. Papanicolaou, and C. Tsogka, *Filtering deterministic layering effects in imaging*, Multiscale Model. Simul., 7 (2009), pp. 1267–1301.

[9] L. Borcea, G. Papanicolaou, and C. Tsogka, *Interferometric array imaging in clutter*, Inverse Problems, 21 (2005), pp. 1419–1460.

[10] L. Borcea, G. Papanicolaou, and C. Tsogka, *Adaptive interferometric imaging in clutter and optimal illumination*, Inverse Problems, 22 (2006), pp. 1405–1436.

[11] L. Borcea, G. Papanicolaou, and C. Tsogka, *Coherent interferometric imaging in clutter*, Geophysics, 71 (2006), pp. SI165–SI175.

[12] M. Born and E. Wolf, *Principles of Optics*, Cambridge University Press, Cambridge, UK, 1999.

[13] M. V. de Hoop and K. Sølna, *Estimating a Green's function from "field-field" correlations in a random medium*, SIAM J. Appl. Math., 69 (2009), pp. 909–932.

[14] A. Derode, P. Roux, and M. Fink, *Robust acoustic time reversal with high-order multiple scattering*, Phys. Rev. Lett., 75 (1995), pp. 4206–4209.

[15] W. Elmore and M. Heald, *Physics of Waves*, Dover, New York, 1969.

[16] J.-P. Fouque, J. Garnier, A. Nachbin, and K. Sølna, *Time reversal refocusing for point source in randomly layered media*, Wave Motion, 42 (2005), pp. 238–260.

[17] J.-P. Fouque, J. Garnier, G. Papanicolaou, and K. Sølna, *Wave Propagation and Time Reversal in Randomly Layered Media*, Springer, New York, 2007.

[18] J.-P. Fouque, J. Garnier, and K. Sølna, *Time reversal super resolution in randomly layered media*, Wave Motion, 43 (2006), pp. 646–666.

[19] J. Garnier, *Imaging in randomly layered media by cross-correlating noisy signals*, Multiscale Model. Simul., 4 (2005), pp. 610–640.

[20] J. Garnier and G. Papanicolaou, *Passive sensor imaging using cross correlations of noisy signals in a scattering medium*, SIAM J. Imaging Sci., 2 (2009), pp. 396–437.

[21] J. Garnier and G. Papanicolaou, *Resolution analysis for imaging with noise*, Inverse Problems, 26 (2010), 074001.

[22] J. Garnier and G. Papanicolaou, *Correlation based virtual source imaging in strongly scattering media*, Inverse Problems, 28 (2012), 075002.

[23] J. Garnier, G. Papanicolaou, A. Semin, and C. Tsogka, *Signal-to-noise ratio estimation in passive correlation-based imaging*, SIAM J. Imaging Sci., 6 (2013), pp. 1092–1110.

[24] J. Garnier and K. Sølna, *Coupled paraxial wave equations in random media in the white-noise regime*, Ann. Appl. Probab., 19 (2009), pp. 318–346.

[25] J. Garnier and K. Sølna, *Wave transmission through random layering with pressure release boundary conditions*, Multiscale Model. Simul., 8 (2010), pp. 912–943.

[26] J. Garnier and K. Sølna, *Cross correlation and deconvolution of noise signals in randomly layered media*, SIAM J. Imaging Sci., 3 (2010), pp. 809–834.

[27] A. Ishimaru, *Wave Propagation and Scattering in Random Media*, IEEE, Piscataway, NJ, 1997.

[28] G. Papanicolaou, L. Ryzhik, and K. Sølna, *Statistical stability in time reversal*, SIAM J. Appl. Math., 64 (2004), pp. 1133–1155.

[29] G. Papanicolaou, L. Ryzhik, and K. Sølna, *Self-averaging from lateral diversity in the Ito–Schrödinger equation*, Multiscale Model. Simul., 6 (2007), pp. 468–492.
[30] G. T. Schuster, *Seismic Interferometry*, Cambridge University Press, Cambridge, UK, 2009.
[31] F. D. Tappert, *The Parabolic Approximation Method, in Wave Propagation and Underwater Acoustics*, Lecture Notes in Phys. 70, Springer, Berlin, 1977, pp. 224–287.
[32] B. J. Uscinski, *The Elements of Wave Propagation in Random Media*, McGraw Hill, New York, 1977.
[33] K. Wapenaar, E. Slob, R. Snieder, and A. Curtis, *Tutorial on seismic interferometry: Part 2—underlying theory and new advances*, Geophysics, 75 (2010), pp. 75A211–75A227.